

1-1-2017

The New Designing Of The Nano-Indentation Method To Applying On The Aisi D-2 Steel

Tangyue Wu
Wayne State University,

Follow this and additional works at: https://digitalcommons.wayne.edu/oa_theses



Part of the [Mechanical Engineering Commons](#)

Recommended Citation

Wu, Tangyue, "The New Designing Of The Nano-Indentation Method To Applying On The Aisi D-2 Steel" (2017). *Wayne State University Theses*. 595.

https://digitalcommons.wayne.edu/oa_theses/595

This Open Access Thesis is brought to you for free and open access by DigitalCommons@WayneState. It has been accepted for inclusion in Wayne State University Theses by an authorized administrator of DigitalCommons@WayneState.

**DEVELOPMENT OF A NANO-INDENTATION SYSTEM AND APPLIED TO AISI D2
TESTING**

by

TANGYUE WU

THESIS

Submitted to the Graduate School

of Wayne State University,

Detroit, Michigan

in partial fulfillment of the requirements

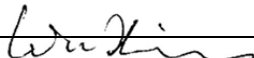
for the degree of

MASTER OF SCIENCE

2017

MAJOR: MECHANICAL ENGINEERING

Approved By:

 7/5/2017

Advisor

Date

© COPYRIGHT BY

TANGYUE WU

2017

All Rights Reserved

ACKNOWLEDGMENT

The master thesis is developed under the advice of Professor Xin Wu, who is passionate for teaching and researching to promote career development of each student. On the first day when I took his class, his researching methods attracted my eyesight. During the course of this thesis development, he provided me many supports from the research idea to the practical approaches, with great endeavor that led me to a correct routine.

I also need to express my great gratitude Pengyan Lu, who is the PhD student of my research group. He provided me samples for the indentation testing, as well as the related micrograph.

Table of Contents

ACKNOWLEDGMENT	iii
List of Tables.....	vii
List of Figures.....	viii
Chapter 1 Introduction.....	1
1.1 Basic principle.....	1
1.2 Development of nano-indentation system.....	2
1.3 Conducting experiment	2
1.4 Organization of this thesis.....	3
Chapter 2 Literature review.....	4
2.1 Parameter of the indenter	4
2.1.1 Elastic properties.....	5
2.1.2 Stress-Strain-Curve	6
2.2 Materials previously studied by indentation method	9
2.3 Microstructure	14
2.4 Algorithm for data processing in experiments	15
2.4.1 Mean filter	16
2.4.2 Fourier Transform.....	16
2.4.3 Wavelet transform	17
2.5 Commercial machine of nani-indentation	18
Chapter 3 Experiment procedure.....	21

3.1	Hardware design.....	21
3.2	Indenter loading-unloading controlling system.....	23
3.2.1	Force dominated controlling mode.....	24
3.2.2	Position dominated controlling mode.....	26
3.2.3	Combined controlling mode.....	28
3.3	Data collection.....	30
3.3.1	Displacement-time wave collection	30
3.3.2	Force-time wave collection	32
3.4	Data processing	33
3.4.1	Filter	33
3.4.2	Force-displacement wave	35
Chapter 4	Experimental results	36
4.1	Microstructure of the material.....	36
4.2	Microscope after the indentation.....	38
4.3	Force-displacement wave for the particles.....	41
4.3.1	Force-displacement wave for the carbide.....	42
4.3.2	Force-displacement wave for the boundaries.....	43
4.3.3	Force-displacement wave for martensite.....	45
4.3.4	Combination of force-displacement wave for particles	46
4.4	Analysis for the material properties for carbide, boundary and martensite	47
Chapter 5	Future work.....	54

Chapter 6 Conclusion	55
APPENDIX	56
REFERENCES	69
ABSTRACT.....	76
AUTOBIOGRAPHICAL STATEMENT.....	77

List of Tables

Table 1.	The stationary for the strain-stress curve in the nano-indentation testing(Ang, Scholz et al. 2009).....	9
Table 2.	The different compositions and features for some selected tooling steels(Karlsson, Gård et al. 2014)	12
Table 3.	The differences among Haar, Mexican Hat and Daubechies wavelet transform	17
Table 4.	The difference of mean filter, Fourier transform and Wavelet transform	18
Table 5.	The difference of force and displacement data collection hardware	19
Table 6.	The parameter of the filter	26
Table 7.	The statistics of the indentation on the carbide, the boundaries and the martensite	40
Table 8.	Number the indentation points by each column and line.....	41
Table 9.	P_{max} , h_{max} , h_c and h_f for the carbide, boundary and the martensite.....	48
Table 10.	The young's modulus, stain and stress for 3 particles for direct force	51

List of Figures

Fig.1.	Load-displacement curve during the loading and unloading period (Oliver and Pharr 1992)	4
Fig.2.	The description of h_{max} (the depth of the indentation in the maximum loading), r (the radius of the indentation in the maximum loading), h_f (the depth of the indentation after the load released) and a (the radius of the indentation after the load released) (Kanari, Tanaka et al. 1997).....	5
Fig.3.	Comparison between the uniaxial compression and indentation for describing the elasticity and plasticity periods(Martínez, Romero et al. 2003)	8
Fig.4.	Microstructure of D-2, with the scale bar in 20 micrometers(Nanesa, Boulgakoff et al. 2016)	13
Fig.5.	The sketch photo for MTS Nano-indenter XP, CSIRO_UMIS(Ultra Micro Indentation System), Hysitron Triboscope and CSM NHT(Nano Hardness Tester)	19
Fig.6.	The hardware designing for the nano-indentation system	22
Fig.7.	The specimen is clamped by the set screw	23
Fig.8.	The flow chart for the indenter loading-unloading controlling system for force dominated controlling mode	25
Fig.9.	Details of collecting and processing the controlling signals for force dominated controlling mode	25
Fig.10.	The flow chart for the indenter loading-unloading controlling system for position dominated controlling system	27

Fig.11.	Details for the signal controlling collect and process for position dominated controlling system.....	27
Fig.12.	The flow chart for the indenter loading-unloading controlling system for the combination controlling system.....	28
Fig.13.	Details for the signal controlling collect and process for the combination controlling system	29
Fig.14.	The interferometric sensor by Attocube FPS 3010	30
Fig.15.	The displacement-time wave collection raw data for 9 loops of indentation read by the MATLAB	31
Fig.16.	The method to collect the voltage-time by using the LabView	32
Fig.17.	The voltage-time wave collection raw data for 9 loops of indentation read by the MATLAB	33
Fig.18.	The displacement-time (left) and force-time (right) waves are filtered by the wavelet transform.....	34
Fig.19.	The force-displacement wave in a completed nano-indentation.....	35
Fig.20.	The microstructure of D2 in 200X (1st), 400X (2nd), 1000X (3rd) and 3000X (4th) microscope (provided by Pengyan Lu)	37
Fig.21.	The microstructure of D2 after indentation in 200X microscope	39
Fig.22.	The indentation force-displacement wave for carbide.....	42
Fig.23.	The force-displacement wave for 10 carbide indentation.....	43
Fig.24.	The indentation force-displacement wave for the boundary.....	44

Fig.25.	The force-displacement wave for 10 boundary indentation	44
Fig.26.	The indentation force-displacement wave for the martensite	45
Fig.27.	The force-displacement wave for 20 martensite indentation.....	46
Fig.28.	The force-displacement wave for carbide (blue), boundary (green) and martensite (red)	47
Fig.29.	h_{max-p} , h_c-p and h_f-p plot for the carbide, boundary and martensite	50
Fig.30.	The strain-stress scatter for the carbide, boundaries and martensite	52

Chapter 1 Introduction

1.1 Basic principle

The material properties are the essential information widely used in mechanical engineering. The material properties, like elastic and plastic properties are determined by microstructures of the material that developed from thermal-mechanical history in material processing. Microstructures of materials are generally not uniform, but contain grains and grain boundaries, and for duplex materials contain different phases and constituents (mechanical mixtures of different phases), and the microstructural configurations give important effect on materials' mechanical properties, including elastic, plastic and fracture properties. Mechanical properties of materials are obtained by various mechanical testing, under different loading conditions and environment, with a wide variety of mechanical behaviors that, for better understanding, require knowledges on microstructure and properties of individual phase and constituents.

The local properties of common engineering materials at the length scales of single phase or constituent can be obtained by nano-indentation method. The nano-indentation is an efficient method to gain the material properties in a proper way. Nano-indentation is a testing method to obtain variety of material properties applied to small volumes.(Poon, Rittel et al. 2008) It is common to use nano-indentation method to test material properties under the indenter that is close to or smaller than the material constituents such as grains and phase particles.

The material properties can be obtained from the load-displacement curve during the loading and unloading period.(Sebastiani, Johannis et al. 2015) Common shapes of the indenter

include Berkovich triangular, conical, spherical etc. Different indenters have different parameters to calculate the material properties.

1.2 Development of nano-indentation system

In this thesis, the nano-indentation system is mainly to determine the elastic and plastic properties for different particles in the same material. In one piece of material, it would include different kinds of particles, which have different kinds of properties. Some lead to the plastic behaviors, some lead to elastic behaviors. By using the tensile test, the plastic and elastic behaviors for different particle is uneasy to determine. However, indent on the particle would produce the loading-unloading curve, which could tell the differences about the particle.

In this study a custom-designed and fabricated nanoindentation system was developed, in which a nanoindenter with 60° conical inclined angle was used instead of Berkovich indenter that is commonly used in commercial nanoindentation systems, for convenience in 2D FEA simulation. Thus, the parameters correlating indentation results to material properties needs to be re-calculated. With the specific parameter for the 60° conical indenter, the strain and stress for different particles can be determined.

1.3 Conducting experiment

To determine the material properties is commonly using the tensile test, bending test etc. For these kinds of testing, it needs to provide a big specimen, which cannot provide local material properties, which are needed to understand the events involving small-scale processing zone, such as fracture. By using nano-indentation system, only small piece of specimen can tell plenty of material information.

Different from other testing, by using nano-indentation, the specimen needs to be polished by using the polisher, examining the micro-structure under the microscope before indent. From the microscope, the area fraction of different particle is easy to be determined. After the indentation, it would put under the microscope again to check the location of indented points and correlate the grains/phases of the locations with the obtained load-displacement curve. To compare the loading-unloading curve with the indentation, the material properties for each point are obtained.

1.4 Organization of this thesis

In this thesis, it is mainly to describe the new designed nano-indentation. This kind of nano-indentation apparatus is much more inexpensive and almost has the same function as compared with the commercial one. The nano-indentation system can get the force-displacement waveform, which is the way to determine the elastic and plastic properties for the particle materials. In the structure, it would describe the designing of the nano-indentation apparatus for a big partial of the thesis. This part is divided into 3 sub-parts: hardware designing, software designing and data processing. The material, AISI D2, is chosen to do the force-displacement measurement, which can determine the plastic and elastic properties.

Chapter 2 Literature review

2.1 Parameter of the indenter

In the loading and unloading curve, the y-axis is for load (P) and x-axis is for penetration displacement (h). In the rest of this document the displacement of indentation curve refers to penetration displacement only. The loading portion of the curve is produced by both elastic and plastic deformation, and the unloading is only the elastic recover. (fig.1). (t with the possibility that during unloading the residual stress may reach yield condition in certain region, for example, many brittle materials develop cracks not in loading but in unloading stage, and this phenomenon has been widely as means of measuring K_{Ic} (fracture toughness) of materials.(Liskiewicz, Kubiak et al. 2017)

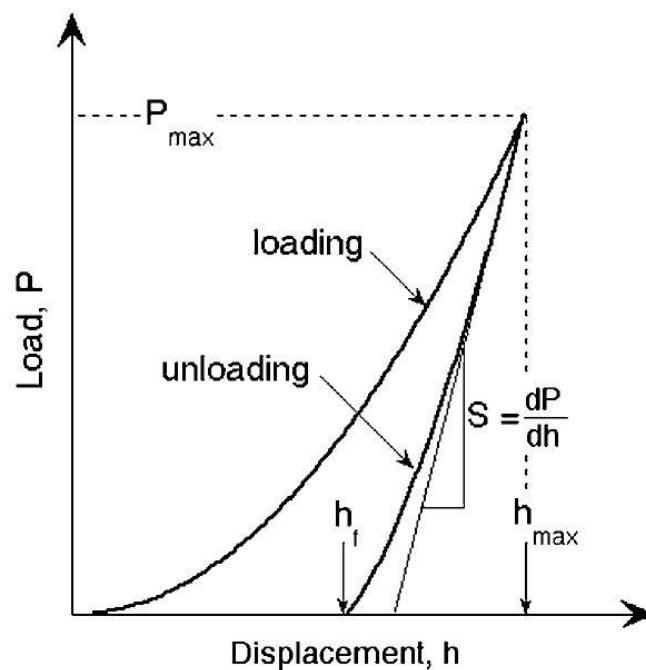


Fig.1. Load-displacement curve during the loading and unloading period (Oliver and Pharr 1992)

2.1.1 Elastic properties

The data subtracted from the curve or obtaining material properties in common analysis are the maximum load, P_{\max} , the maximum displacement, h_{\max} . Then by using the unloading curve, the elastic stiffness is:

$$S = \frac{dP}{dh} \quad (1)$$

Another data point needs to be read is h_f , which is the permanent penetration depth after the unloading.

In the nano-indentation testing, it is necessary to determine the contact area. The contact area is the projected area along the indenting direction when the indenter is fully loaded. It is estimated from the depth of the penetration with the know geometry of the indenter. (Machaka, Derry et al. 2014, Tiwari and Hihara 2014)

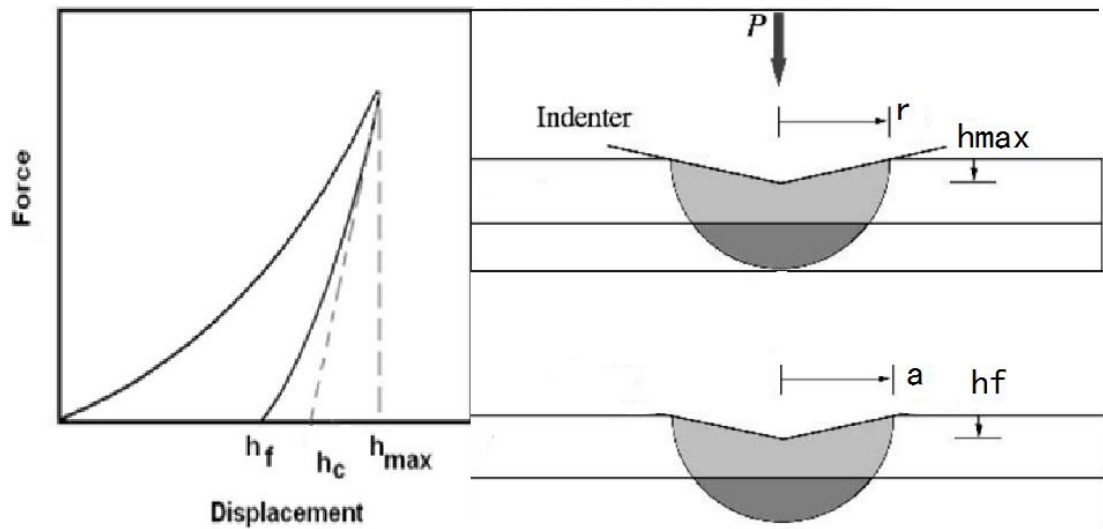


Fig.2. The description of h_{\max} (the depth of the indentation in the maximum loading), r (the radius of the indentation in the maximum loading), h_f (the depth of the indentation after the load released) and a (the radius of the indentation after the load released) (Kanari, Tanaka et al. 1997)

In the Fig 2, the h_c is the height when the indenter has the maximum contact area with the specimen. To get h_c , the fitting curve (describe fit what equation) would only chooses the top 25% to 50% of the unloading curve. [3] The contacted area for the conical indenter is related to the a , h_c and h .

$$A_c = 2\pi ah_c; A_f = 2\pi ah_f \quad (2)$$

The hardness, H , would be calculated as:

$$H = \frac{P_{\max}}{A_f} \quad (3)$$

The indenter and the specimen's effective elastic modulus is from the formulation of elastic stiffness S as.

$$S = \beta \frac{2}{\sqrt{\pi}} E_{\text{eff}} \sqrt{A_c} \quad (4)$$

where E_{eff} (effective elastic modulus) is given in reciprocal form as:

$$\frac{1}{E_{\text{eff}}} = \frac{1-\gamma^2}{E} + \frac{1-\gamma_i^2}{E_i} \quad (5)$$

where γ and E are the Poisson's ratio and the elastic modulus of the chosen materials, and γ_i and E_i are the Poisson ratio and the elastic modulus for the indenter.

The β in the Eq. 4 is the correction factor that depends on the geometry of the indenter. Hay (Hay, Bolshakov et al. 1999) used finite element analysis to develop an equation which is related with the half included angle and the Poisson's ratio of the indenter.

$$\beta = \pi \frac{[\frac{\pi}{4} + 0.1548 \cot \varphi \frac{1-2\gamma_i}{4(1-\gamma_i)}]}{[\frac{\pi}{2} - 0.8312 \cot \varphi \frac{1-2\gamma_i}{4(1-\gamma_i)}]^2} \quad (6)$$

the φ is the half-angle of the indenter's top, γ_i is the Poisson's ratio of the indenter.

2.1.2 Stress-Strain-Curve

Different from the result from the uniaxial testing, the nano-indentation would test

different penetration depths of the loading and unloading periods to get the strain and stress, and then link these strain-stress point together.(Kim, Ahn et al. 2015) In Fig.3(a), the true stress-strain for the uniaxial testing is divided into elastic and plastic regions. The linear line of the beginning of the testing is the elastic period, and after yielding point, the plastic portion appears.(Pradeepkumar, Sibin et al. 2015) However, for indentation that involves continuous increase in deformation zone that experiences elastic and plastic deformation so that the elastic deformation never complete the majority portions of the H-R curve are within elastic-plastic condition except at beginning only small initial portion is within fully elastic deformation, and after large penetration the plastic deformation becomes more dominating. As described by Fig.3(b), the three regimes were considered: the elasticity, elasticity-plasticity and plasticity periods during the loading period. The beginning of the H-R curve is linear behavior, which represents the elastic periods. The end of the elastic period is the initial yielding, which is the beginning of the elastic-plastic period. The stationary yielding point connects with the elasticity-plasticity and plasticity periods. (Fisher-Cripps 2000)

Note that in Fig.3(b), the H-R curve is not only suitable for the ball-shape indenter, but for any kinds of indenters as well.

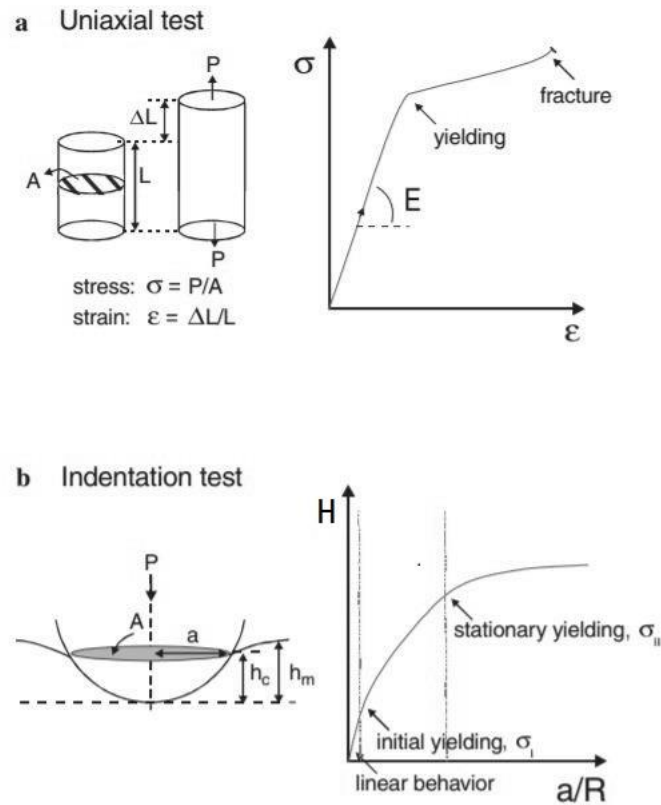


Fig.3. Comparison between the uniaxial compression and indentation for describing the elasticity and plasticity periods(Martínez, Romero et al. 2003)

The indentation stress is applied on the force-displacement curve (Fig. 2). Each point on the loading and unloading curve has the stress. For each point, the parameter of force and depth could be read, which calculates the stress from the force and area. stress = force/area.

During the indentation, the indenter dips a hole for some volume, and develops a plastic zone and an elastic zone behind it.(Chen, Wang et al. 2014) To determine the influenced volume is not easy, thus by using the FEA model, the indentation strain is almost related a and R.

$$\varepsilon = \frac{a}{R} \quad (7)$$

a is the reminding radius of the hole when the force is released. R is the radius of the hole when the force is applied on the specimen.

Now, back to the Fig. 3(b), the H-R curve is divided into 3 zones. Y is the initial yielding stress; E is the elastic modulus. When stress is smaller than the $1.1Y$, it is the elastic deformation. When stress is over $1.1Y$ and smaller than CY , it is the elasticity-plasticity zone. C is dependent to the specimen material and indenter type used, and based on different studies it was suggested that $C = E/Y$ for the metal (Hutchings 2009), usually $C = 1.5$ (Swain and Hagan 1976). When stress is over CY , it is plastic deformation.

Table 1. The stationary for the strain-stress curve in the nano-indentation testing (Ang, Scholz et al. 2009)

Stationary	Conditions	Notes
Elastic deformation	$<1.1Y$	
Elastic and plastic deformation	$1.1Y \sim CY$	Y is the compressive yielding stress; C is 1.5 for most materials
Plastic deformation	$>CY$	

For most materials, the first period is the linear condition, which is the elastic period. The indentation is able to be recovered from this station. After the linear periods, it is the elastic and plastic period. The indentation could be recovered some portion when contrasts with the maximum loading. Finally, the indentation in the plastic period would be recovered most portions.

2.2 Materials previously studied by indentation method

In this review, we limit the materials to testing the force-displacement curve. In this condition, the material with big particle size is essential to be verified, which is easy to be determined under the microscope. The microstructures before and after the indentation should

figure out whether the indent on the particle or on the edge.

AISI-D2 steel is a commonly used steel. It contains high carbon and a variety of alloying elements, which through certain heat treating process (quenching), form carbide particles and martensite matrix, both are at high strength and hardness. The material particularly suitable for tool application. (Shyi-Ming 1997) Their suitability of this material for tool application comes from this very high hardness, resistance to abrasion and deformation. As a trim die material it can hold a high compression and chipping stress at the cutting edge. (Starling and Branco 1997) The tool steel includes the water-hardening group, cold work group, shock-resisting group, high speed group, hot-working group etc. (Antretter and Fischer 1997)

W-group is the water-hardening group. W-group tool steel gets its name from its defining process of having to be water quenched, which is the high carbon plain-carbon steel. This kind of material is low cost than other kinds of materials. These steels can attain high hardness but relatively brittle to compare with other tool steels. (Choudhury and Chinchankar 2017)

D2 belongs to the cold-work class of tool steels. This class of tool steels can be further classified to a few series: the O-series (oil-hardening), the A-series (air-hardening), and the D-series (high carbon-chromium). In O-series, it has O1, which is used to cut tools, woodwork the knives. (Liverani, Lutey et al. 2016) In A-series, the family has 8 steel, they are A2, A3, A4, A5, A6, A7, A8, A9 and A10. For these materials, the machinability is good and they are balanced wear resistance and toughness. (Watanabe, Arase et al. 2016) In the D-series, it includes D2, D3, D6 and D7. The D-series steel is the stainless or the semi-stainless steel. Their corrosion resistance is limited because the carbide precipitation of the majority of carbon

constituents.(Spangel, Matthaeci-Schulz et al. 2002)

With the excellent high temperature strength, D2 can be used for the shear blade, planer blade and cutting tools. (Conci, Bozzi et al. 2014)

Different from O series and A series tool steels, D series steel has more chromium and carbon constitutes as carbide, which makes the structure harder.(Hamilton, Wood et al. 2013)
The selection of the O-series, A-series and D-series steels need to consider combination of their chemical the compositions, manufacturing processes, working conditions and material performance.(Cho, Song et al. 2014) Table 2 summarized and compared the compositions and characteristics of O-1, A-2, A-6 and D-2.

Table 2. The different compositions and features for some selected tooling steels(Karlsson, Gård et al. 2014)

Steel	Compositions	Features
O-1	0.90% C,1.0–1.4% Mn,0.50% Cr,0.50% W	It is a cold work steel; it is hard to be made for wood-cutting tools and knives.(Badkar, Pandey et al. 2010)
A-2	1.0% C,1.0% Mn,5.0% Cr,0.3% Ni,1.0% Mo, 0.15–0.50% V	It is a common general purpose tool steel; it is not so hard; thus, it is commonly used for different kinds of forming punching, trimming and rolling. (Paul and Strano 2016)
A-6	0.7% C,1.8–2.5% Mn,0.9–1.2% Cr,0.3% Ni, 0.9–1.4% Mo	It is air-harden steel which is operated at a very low temperature. Therefore, it is a stable material which is used for high resistance works.
D-2	1.5% C,11.0–13.0% Cr;0.45% Mn,0.030% P, 0.030% S, 1.0% V, 0.9% Mo, 0.30% Si	It is high resistance but low tough material, and it is sensitive to the heat treatment. It is hard and stable to build shear blade, industrial cutting tools.(Staia, Pérez-Delgado et al. 2009)

AISI D-2 is a widely used tool steel used for forming dies and cutting tools. It consists of

large carbide particles and martensitic matrix after air quench, see Fig 4 as an example. Based on this figure, it estimates that there are 70% martensite and 30% carbide.

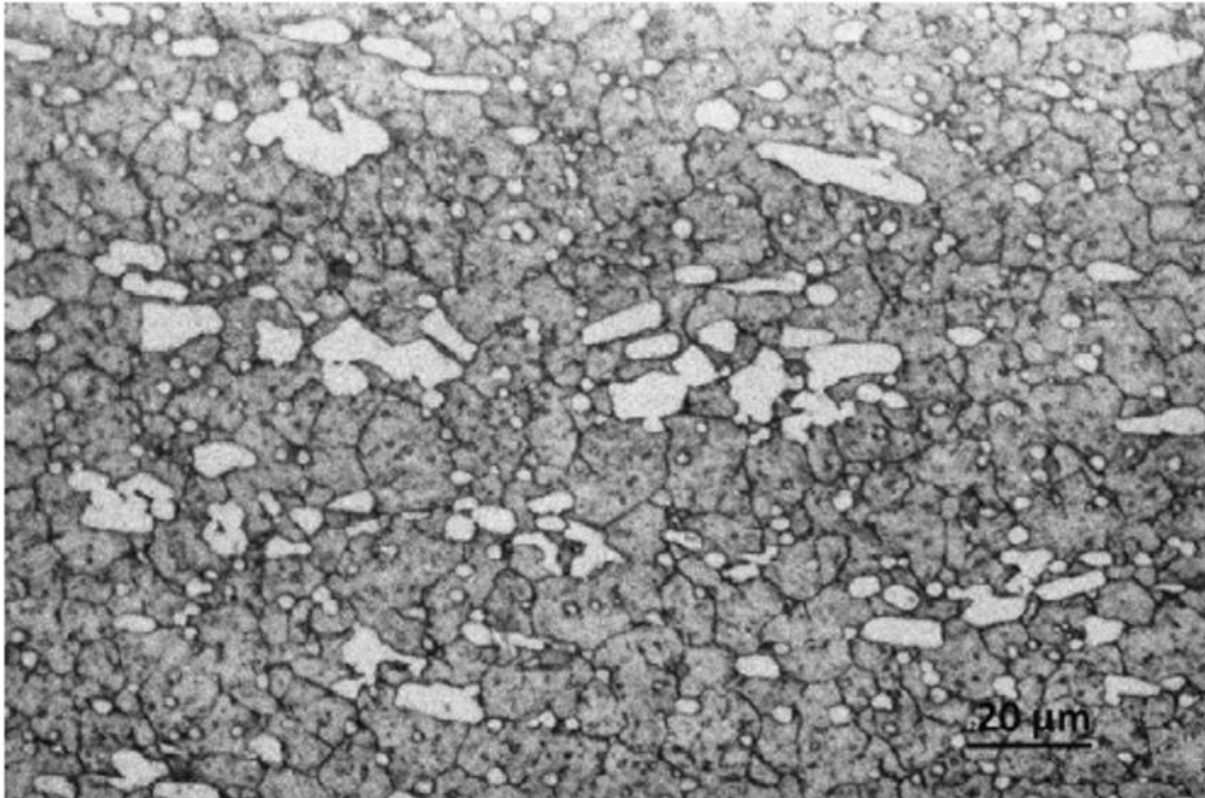


Fig.4. Microstructure of D-2, with the scale bar in 20 micrometers(Nanesa, Boulgakoff et al. 2016)

It shows the benefits from the cryogenic cooling to the grinding of the AISI D2 steel are completely belong to the conventional oil-based grinding fluid.(Sam Paul, Varadarajan et al. 2016) The effect of heat treatment parameters on the dimensional stability of AISI D2 has been studied by.(Stratton, Surberg et al. 2008) On AISA D2 as base tool material and with additional surface coating, the tool performance received further improvement: the application of the cutting specimen can reduce the grinding force and improve the surface roughness, reduce the damages and lower the tensile residual stresses.(Okonkwo, Kelly et al. 2012, Saba, Kabiri et al. 2016)

2.3 Microstructure

In 2.2, the microstructure has been noticed which could determine the structure of the materials. It could show different particles, the range of the particles and particle size for the specimen.

Microstructure is micro-scale structure of a material, which is in the prepared surface for the specimen. The microstructure is observed in the microscope above 25× magnification. The microstructure of a material will affect many properties, such as hardness, modulus of elasticity, strength, toughness etc. The microstructure would influence on the mechanical and physical properties of a material. It is primarily governed by the different particle present or absent of the structure.

The microstructural features it to give material greatly when it observes at different length scales. For this reason, it is necessary to consider the length scale of the observations when describing the microstructure of a material.(Fukai and Ando 2004)Importantly, microstructure affects the physical properties and behavior of the material, and it is able to give the specific properties of the material. Among the microstructure control processes, one important material strengthening process for tool steel is thermal treatment, more specifically the austenite to martensite phase transformation, see one of such studies by Hane et al.(Hane and Shield 2000)

The microstructures of materials are commonly observed by various kinds of microscopies. The optical microcopy uses commonly in the experiments. The specimen is well prepared, such as: cutting, microtomy, polishing, etching, vapor-deposition etc.(Liu and Mandler 2014) It is widely used in many materials like metal, ceramics, glass, compositions

and so on. The X-ray microscopy is commonly used in biology and medical research. It is very expensive not only in apparatus but also in maintenance. Through 2D microstructure knowledge a 3D microstructure may be speculated. Electron microscopy directly observes the atomic-scale features such as grain boundaries, dislocations and so on. It is mainly used on solid state material. The modern atomic force microscopy.(Yu, Burnham et al. 2015) Unlike other method, this technology needs the minimum preparation of the specimen, thus is perfect for studying nanomaterials and a single atom resolved technique. In recent years significant progress has been made in direct 3D imaging technique, even at nanoscale, with the use of electron microscopy based quantitative and analytical 3D tomography, see a review article by (Ersen, Florea et al. 2015).

In Fig.4, it is the microstructure for AISI D-2 steel, most of the carbide particles (in light color) is at the area size over $100\mu\text{m}^2$. The volume fraction, particle size and distribution pattern of the carbide in the martensite matrix are important microstructure features that affect the overall mechanical properties and performance of the material. Quantitative metallography is the measurement and analyzing tool for microstructure study. To better understand the mechanical properties of D2 material, a microstructure and micro-mechanical information are important, in particular the phase and grain size distribution and mechanical properties of individual constituents (carbide particles and martensite matrix).

2.4 Algorithm for data processing in experiments

In our experiment, the force-time curve and displacement-time curve are raw data, which have many noises over the true signals. In this condition, signal processing is used to get true

signal by filtering noises. Here three kinds of filtering techniques that were used in this study are described, namely: mean filter, Fourier filter and wavelet filter, to denoise the signal.

2.4.1 Mean filter

The mean filter is a simple sliding-window spatial filter that replaces the center value in the window with the mean of all the values in the window.(Liu, Chen et al. 2015) The mean filter is one of the simplest ones in signal processing, which will make the processing pace quick. However, using the mean filter would have the most distortion, when the frequency of the noise is low. In this condition, the noise would remind with converting signal. Thus, this filter is suitable for very high frequency noise. An adaptive nonlocal means filter algorithm was use by in reduction of laser speckle in image process. (Dong-hai, Yue-song et al. 2014)

2.4.2 Fourier Transform

The Fourier Transform is helpful to de-noise the signal. When it gets the sound, or gets the change of the load or vibration of the material, for example, it uses the signal to identify the phenomenon (Chen 2014) used this method in Fourier transform profilometry, and used Fourier transforms for noisy 2D signals in the data processing.(Chen, Su et al. 2005)

Short time Fourier Transform(STFT) usually de-noise the signal. It is based on the Fourier Transform to observe the frequency. Different window length will be used to study the effect of resultant resolution in the time and frequency domain. Different window type such as rectangular, Gaussian, and Hamming windows can be used to process the same signal with different de-noised effect. By using the rectangular window, the noise is obvious at the edge of the window.(La Torre and Vrscay 2014) However, the Gaussian, and Hamming windows would

be better to de-noise the signal in the meantime. In addition, the impact of the Filter Bank Summation(FBS) constraint will be examined on synthesizing time varying signals.(Djurović and Stanković 2012)

2.4.3 Wavelet transform

The wavelet transform is to convert signal into another form which either makes certain features of the original signal more amenable to study or enables the original data set to be described more succinctly. It is similar to the Fourier Transform, the Wavelet Transform can also have the continuous wavelet transform (CWT) and discrete wavelet transform (DWT).(Ugweje 2004)

There are about 15 kinds of wavelet in MATLAB. They are like Haar, Mexican Hat, Daubechies, Morlet, Meyer and so on.(Anoop Suraj, Francis et al. 2014) For this project, we mainly discuss the Haar, Mexican Hat and Daubechies wavelet transform.(Yang 2014)

Table 3. The differences among Haar, Mexican Hat and Daubechies wavelet transform

	Haar	Mexican Hat	Daubechies
Form	haar	mexh	db N
Orthogonal	Y	N	Y
CWT	Y	Y	Y
DWT	Y	N	Y
Filter length	2	[-5,5]	2N
Symmetry	Y	Y	Almost

Table 4. The difference of mean filter, Fourier transform and Wavelet transform

	Mean filter	Fourier transform	Wavelet transform
Speed	Fast	Slow	Medium
Correction	Low	High	High
Hardware requirement	Low	High	Medium

In this circumstance, the mean filter is suitable in the system controlling, because during the system controlling, it needs fast speed and the frequency of the noise is low. However, during the data processing, the wavelet transform provides the high corrections and occupy medium hardware resource. The Daubechies filter among wavelet transform would offer high corrections for the complicated wave. Thus, mean filter and Daubechies wavelet are processed in system control and data processing.

2.5 Commercial machine of nani-indentation

Several kinds of nano-indentation machine are sold in the market and four typical are: MTS Nano-indenter XP, CSIRO_UMIS(Ultra Micro Indentation System), Hysitron Triboscope and CSM NHT(Nano Hardness Tester). (Fig.5) (<https://www.slideshare.net/viet4777/nano-indentation-lecture1>)

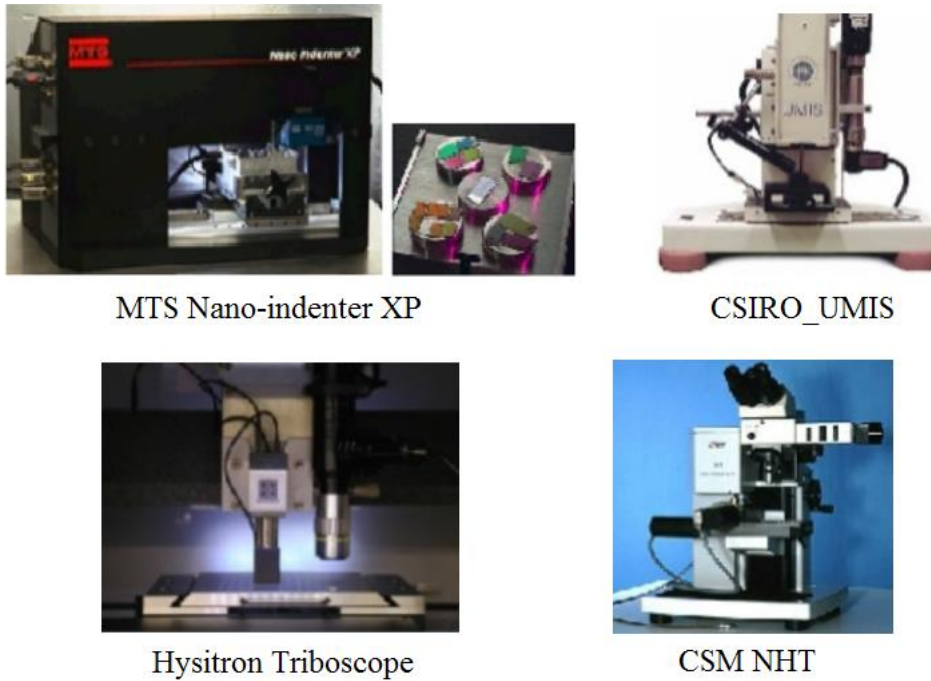


Fig.5. The sketch photo for MTS Nano-indenter XP, CSIRO_UMIS(Ultra Micro Indentation System), Hysitron Triboscope and CSM NHT(Nano Hardness Tester)

The force and displacement data collection is different among these machines. Table 5 gives the various hardware differences.

Table 5. The difference of force and displacement data collection hardware

	Force measurement hardware	Displacement measurement hardware
MTS Nano-indenter XP	Inductive force generation system	Capacitance gage
CSIRO_UMIS	Leaf spring	Force LVDT
Hysitron Triboscope	Two perpendicular transducer system	Center plate capacitive measurement
CSM NHT	Electromagnetic actuator	Capacitive measurement

Although these commercial machines have different data collection measurements, they

are very expensive. In this experiment, the new designed nano-indentation system would be established which cost low expense and acceptable accuracy.

Chapter 3 Experiment procedure

This experiment procedure is mainly divided into three sections i.e. hardware designing, indenter loading-unloading controlling and data processing. Firstly, load cell and interferometric sensor are connected by the micro-motor and NI to get the force and displacement. Then, the indenter loading-unloading controlling system is utilized to indent and forward the specimen. Finally, several data processing filters are applied to the collected data to obtain the force-displacement curve. In addition, the 60° conical shape indenter is used in this experiment.

3.1 Hardware design

As shown in Fig.6, 2 manually forward and back adjustments, 1 manually up and down platform, 1 rotation adjustment, 1 load cell, 2 micro-motors and 1 interferometric sensor are assembled and implemented in this experiment. The 2 motors is operated the y-axis up and down and x-axis forward and back. The manually forward and back adjustments adjust the specimen into the experimental area. The manually up and down platform moves the indenter into the directed height. The rotation adjustment rotates the specimen into the experimental area. The interferometric sensor and the load cell separately measure the displacement and the force.

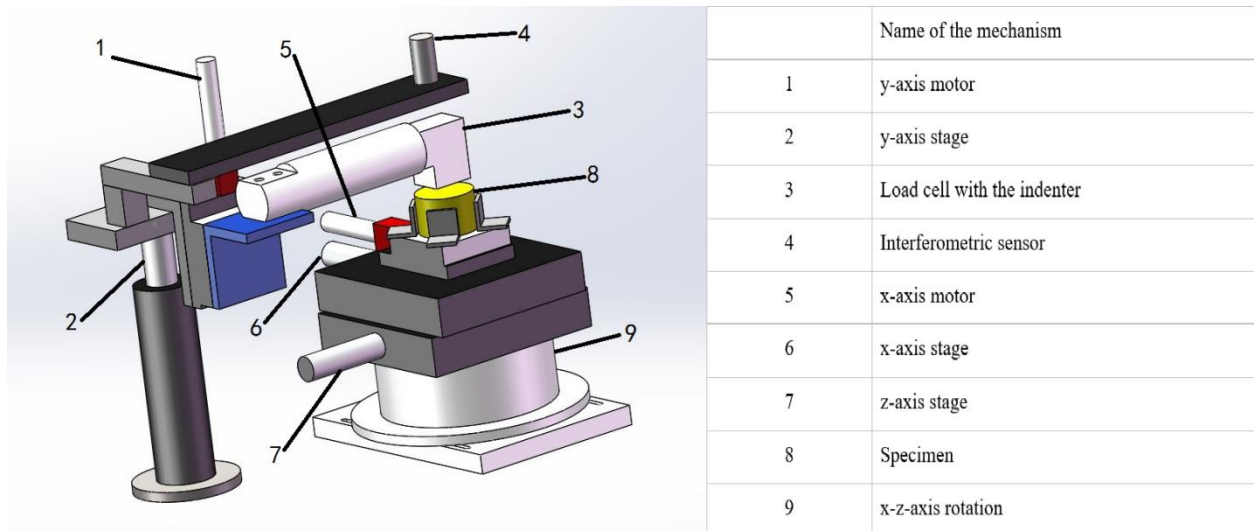


Fig.6. The hardware designing for the nano-indentation system

Before performing the experiment, it needs to use the manual adjustment to set the specimen into the testing area and the indenter into the proper height, which means almost contact with the specimen but not reaching. When y-axis motor goes down, the load cell begins to continually detect whether the force reaches the setting value or not, which is used as a signal to trigger the interferometric sensor measuring the displacement. If the load cell reaches the setting value, the y-axis motor would go up to the original height, then the x-axis motor forwards one step.

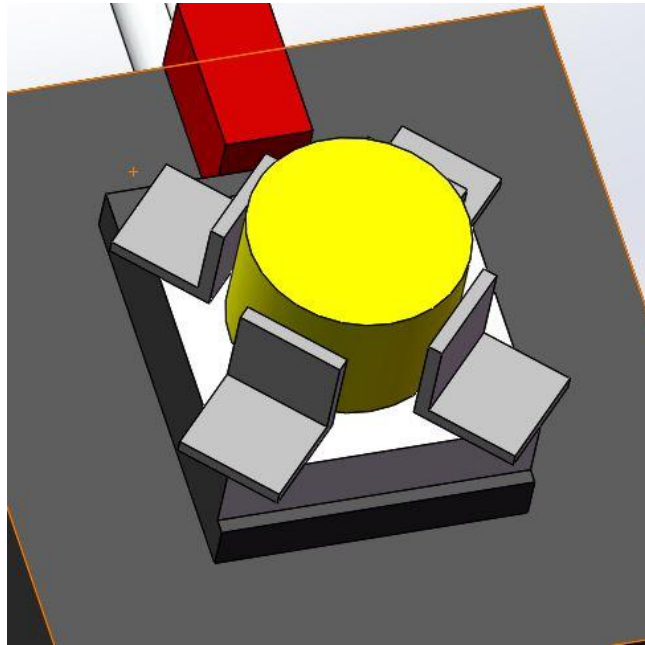


Fig.7. The specimen is clamped by the set screw

As seen from Fig.7, the specimen is clamped by the set screws aiming to avoid the indenter pulling the specimen in the unloading period. If there is no this kind of restriction, the force and displacement curve would show big vibration at the end of the unloading stage.

Under this hardware designing, the controlling and data collection would be discussed in the following section. And the model of the hardware and geometry of the indenter will be described detailedly in section 4.3.

3.2 Indenter loading-unloading controlling system

In the motor movement controlling system, three hardware components i.e. load cell, x-axis step motor and y-axis step motor are linked in terms of the sequential software design. The function of y-axis step motor is indenting the specimen, while that of x-axis step motor is forwarding one point to another point. During the trail test, three different kinds of controlling system are compared i.e. force dominated mode in which force is used to control the system, position dominated mode in which displacement is used to control the system and

combination controlling mode in which both force and displacement are used to control the system. It is obtained that the force dominated controlling mode is accurate but slow, and that the position dominated controlling mode is fast but inaccurate. However, the combination controlling mode is faster than the force domain mode and more accurate than the position domain mode. Thus, the combination controlling mode is the optimistic method in this experiment.

3.2.1 Force dominated controlling mode

The schematic flow chart for the indenter loading-unloading controlling system in force dominated controlling mode is shown as Fig.8. In the loading stage in which the detected force hasn't reached the setting value, the load cell would trigger the y-axis motor to step down periodically. Once the force achieves the setting point, the indenter will turn into the unloading reign in which the y-axis motor would continuously move up to the original position. Because it needs feedback from the load cell to determine the next motion of the y-axis motor, the force dominated mode is indeed slow. Furthermore, the DC motor is used to simulate the step motor in this test, in which the y-axis motor jogs 0.5 micrometer per time and the x-axis motor forward 10 micrometers per time.

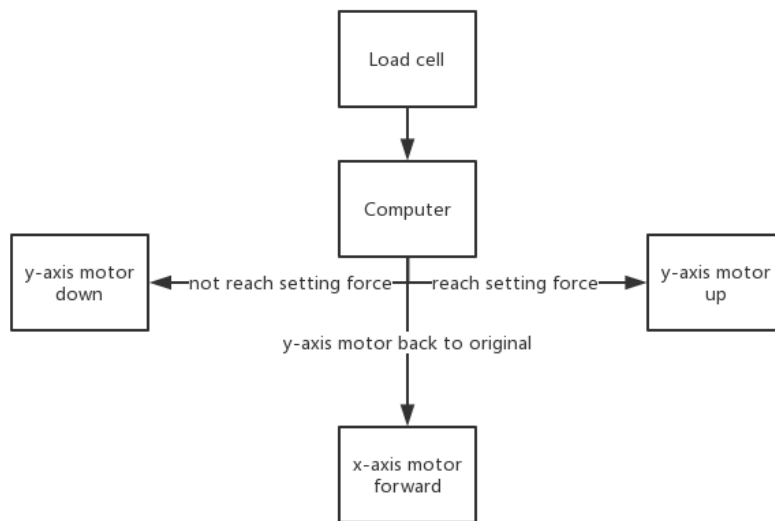


Fig.8. The flow chart for the indenter loading-unloading controlling system for force dominated controlling mode

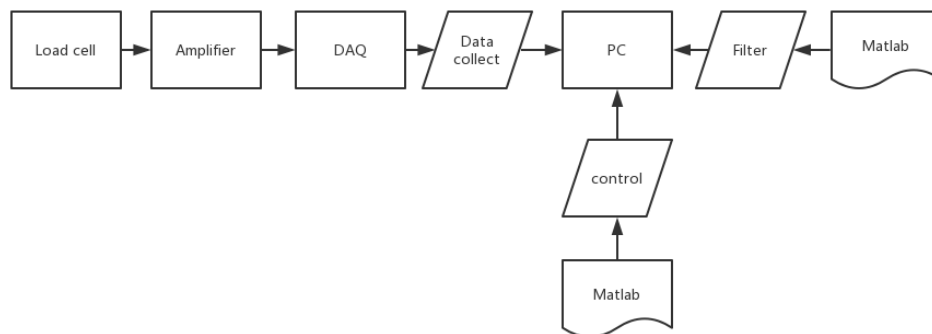


Fig.9. Details of collecting and processing the controlling signals for force dominated controlling mode

Fig.9 is the details of collecting and processing the controlling signals for force dominated controlling mode corresponding to the 'computer' module of the Fig.8. As seen from Fig.8, the controlling mode is operated by the MATLAB software where GUI is used as the guide to set the control button to start, pause and stop the indentation. The force signals which have been amplified by the amplifier are collected by the data acquisition(DAQ).

Because the low frequency leads to the lower accuracy while the high frequency generates the slower processing speed, the frequency of DAQ needs to be adjusted to certain level to avoid these two deficits. As shown in table 5, the frequency of the DAQ is selected as 10000Hz, then the first 1000 data points are imported into the mean filter. By using this filter, not only the processing speed will be quicker but the estimation will be faster.

Table 6. The parameter of the filter

DAQ Frequency	10000Hz
Data points imported into filter	1-1000
Filtering	Mean

By obtaining the flow chart of Fig.9 and filter parameter of table 6, the controlling mode loops by the turns of data collection, filtering and controlling.

3.2.2 Position dominated controlling mode

The position dominated controlling system has some differences with the force domain controlling system.

As shown in Fig.10, when the indenter doesn't reach the setting position, the y-axis motor would move down, on the contrary, the motor would go back to the original position and x-axis motor would forward one step. Thus, in the position dominated controlling system, the y-axis motor moves continuously both up and down. Based on this condition, the indentation speed is much faster than the force dominated controlling system.

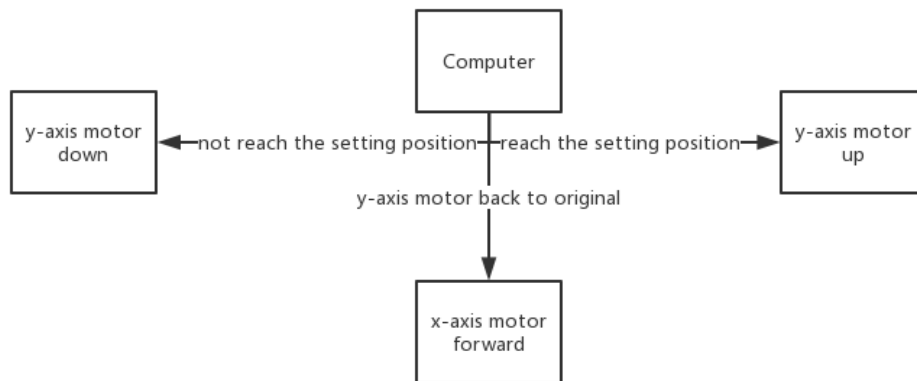


Fig.10. The flow chart for the indenter loading-unloading controlling system for position dominated controlling system

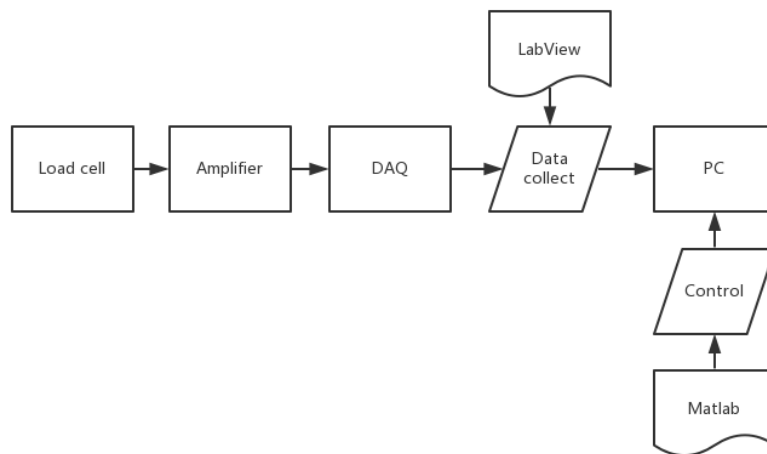


Fig.11. Details for the signal controlling collect and process for position dominated controlling system

In addition, as shown in Fig.11, the position dominated system uses LabView to collect the data. The Labview is capable to show the signal, which is the main difference from the force domain controlling system as the data can be filtered after the whole data has been collected. By using this way, it would improve the speed of the signal collection tremendously. Overall, the indentation speed of position dominated controlling system is

hundreds of times faster than that of force dominated controlling system.

3.2.3 Combined controlling mode

Although the position dominated controlling system speeds up the data collection a lot, it is impossible to control the load condition during indentation. In order to solve this issue, a combined system is adopted in this study.

As shown as Fig.12, the combination controlling system which consists of the force domain and position domain controlling mode would make the data collection both fast and accurate, because it inherits the advantage of quick data collection and can monitor the load as well.

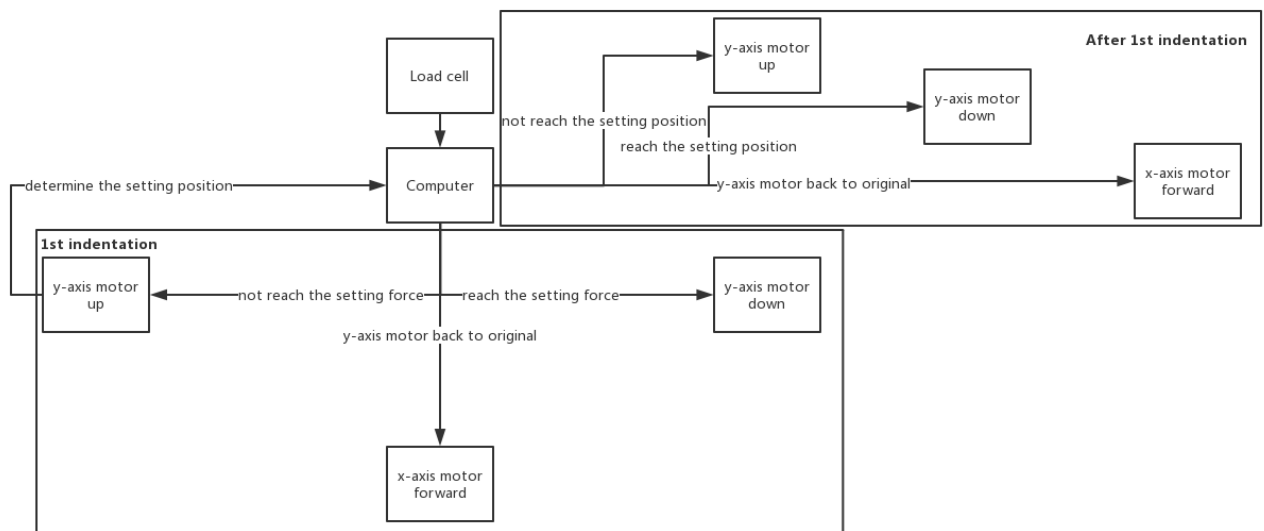


Fig.12. The flow chart for the indenter loading-unloading controlling system for the combination controlling system

Specifically, in the 1st indentation, the combined controlling system collects the force data as force dominated controlling system does. Meanwhile, the position where the force reaches the setting value is used as the reference point for the rest of indentations controlled

by position dominated system.

By using this method, the filter used in data acquisition(DAQ), causing the low speed, would not participate in the controlling from 2nd indentation. Thus, the 1st indentation is called the pilot, which is to determine the position for the rest of the indentations.

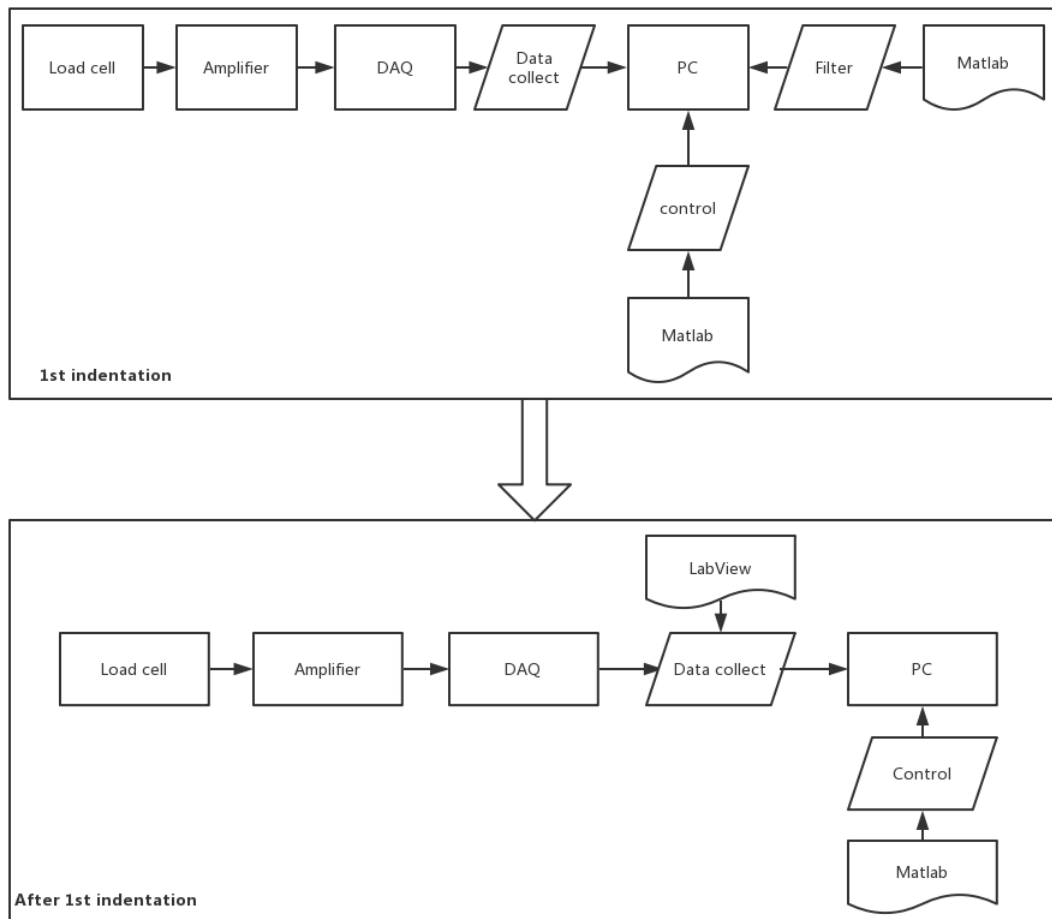


Fig.13. Details for the signal controlling collect and process for the combination controlling system

Fig.13 shows the details for the signal controlling collect and process for the combination controlling system. The 1st indentation is like force dominated system, which uses MATLAB to control the system and filter the data. After the 1st indentation, it would be

processed by the position dominated system, which would be much faster. Therefore, using this kind of controlling system, it would get data fast and accurate.

3.3 Data collection

The nano-indentation is mainly aimed to gain the force-displacement curve. In this experiment. Firstly, the force-time curve and the displacement-time curve are generated from the load cell and interferometric sensor respectively. Then using the same time line, the force data and displacement data are correlated together to get the final force-displacement curve.

3.3.1 Displacement-time wave collection

The interferometric sensor would help to collect the displacement-time wave. As showed in Fig.14, this experiment chooses the Attocube FPS 3010 interferometric sensor to directly collect the signal.



Fig.14. The interferometric sensor by Attocube FPS 3010

Before measuring the displacement, it needs to properly adjust the distance between mirror and interferometric sensor to make the length measurement accurate. When the detected signal is over the range of the referenced line, the displacement signal could be used.

The frequency for the signal is set as 1000Hz, which is as same as the force-time wave. There is box which shows the Fourier Transform wave for the displacement signal. When the signal is stable, which means the wave is in the low frequency, the displacement signal could be collected.

After clicking the recorder button, the signal would be written as the txt files. The MATLAB would read this txt file, and the raw data for 9 loops of indentation is presented in Fig.14.

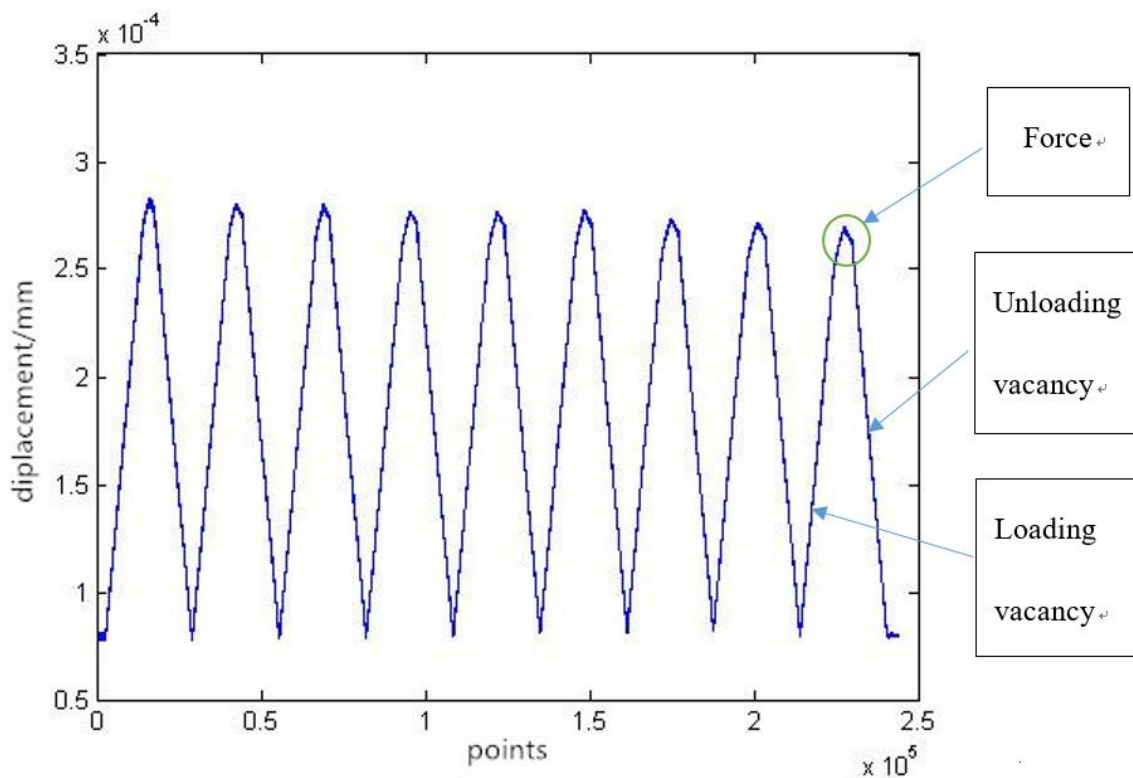


Fig.15. The displacement-time wave collection raw data for 9 loops of indentation read by the MATLAB

In Fig.15, it is obvious that the indenter is from the vacancy to loading and unloading to the vacancy. After it is de-noised, the wave would be the displacement-time curve of the nano-

indentation system.

3.3.2 Force-time wave collection

The force-time wave is from the voltage-time signal, which comes from the national instrument(NI). As this experiment uses the combination controlling system, the signal would be presented on the LabView's wavebox. As showed in Fig. 16, the LabView signal is originally from the DAQ Assistant 2, where the terminal configuration is set as RES, the acquisition mode is selected as continuous samples, sample to read is chosen as 1, and the frequency is used as 1000Hz. Then, the DAQ is connected to configure converter which selects the waveform and exports the its graph to front panel. By using this simple LabView program, the wave data could be collected visually.

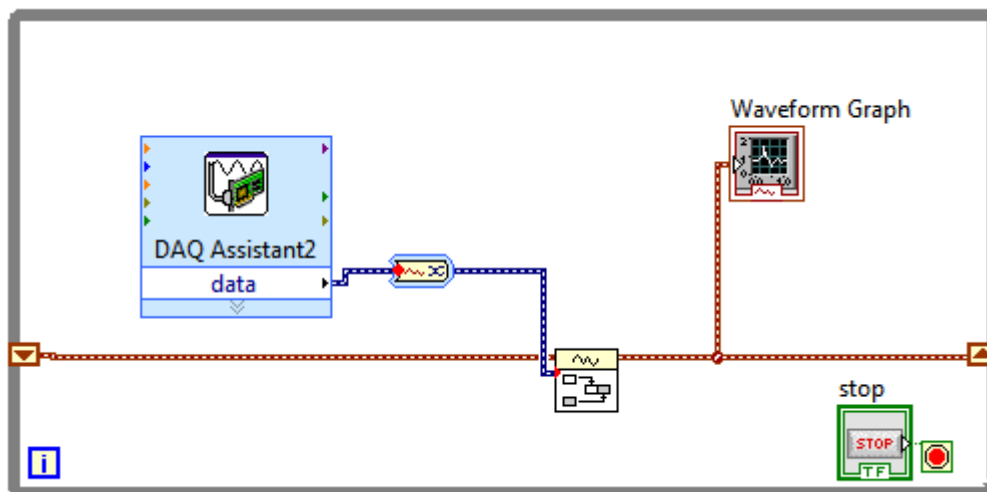


Fig.16. The method to collect the voltage-time by using the LabView

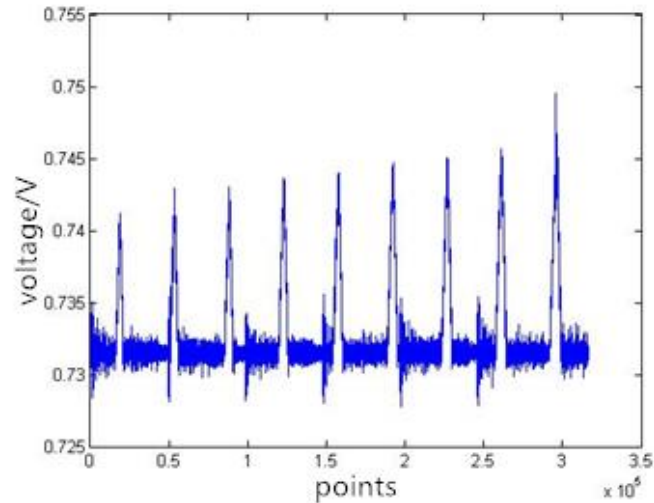


Fig.17. The voltage-time wave collection raw data for 9 loops of indentation read by the
MATLAB

The raw voltage-time data for 9 loops of indentation is presented in Fig.17. The voltage data is firstly converted to the force by a factor of 16100mN/V. After conversion and denoising, the force-time wave is obtained.

3.4 Data processing

Due to the limitation of random access memory(RAM), only 9 completed indentation loops under the combined controlling system can be recorded one time, which means it would obtain 9 force-displacement curves correspondingly. These 9 points is in one line and the indenter moves forward the distance of 100 μm . The collected raw data of displacement-time and force-time is put into the filter to denoise firstly. Combining force-time curve with the displacement-time curve by using the same time axis, the force-displacement curve i.e. the nano-indentation curve is then established.

3.4.1 Filter

In this experiment, the raw data of the displacement-time and force-time is demonstrated

as wave, so the wavelet transform is adopted to denoise. The wavelet transform is to convert signal into another form which either makes certain features of the original signal more amenable to study or enables the original data set to be described more succinctly. It uses the dB4 and level 7 to de-noise the wave. Fig.18 is a typical graph of filtered displacement-time and force-time curves by wavelet transform.

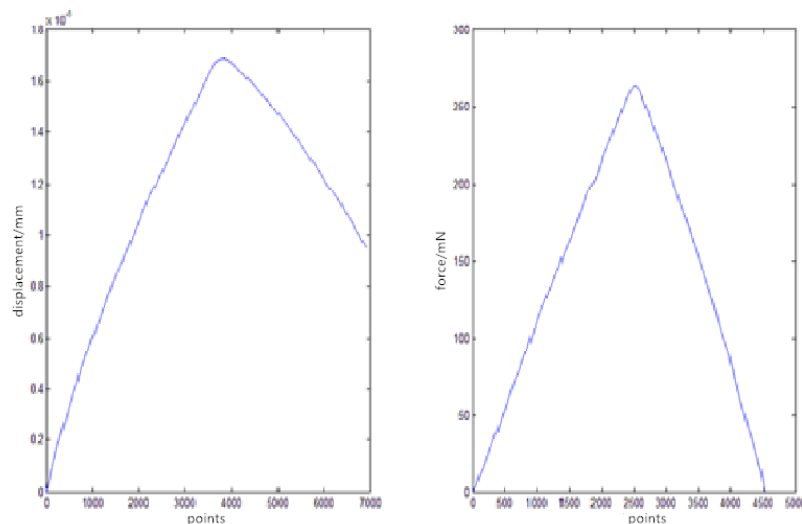


Fig.18. The displacement-time (left) and force-time (right) waves are filtered by the wavelet transform

The displacement-time and force-time waves including 9 whole loops are respectively divided into 9 individuals according to the same time axis. After the wavelet transform and the elimination of vacancy indentation, the plotted image(Fig.18) is the loading and unloading phase for the displacement-time and force-time wave. As the force is symmetric in both loading and unloading while the displacement is not, it is easy to conclude that some plastic deformation should occur after nano-indentation. The detailed analysis would be discussed in the following paragraph.

3.4.2 Force-displacement wave

As it has noticed, the force-displacement wave would be combined with the force-time wave and displacement-time wave by using the same time axis.

Mostly, the time axis in the both waves is different, thus the longer wave has to mean the points in order to make the time axis to be the same length. Then the force could correspond to the displacement. Fig.18 is the force-displacement wave in a completed nano-indentation.

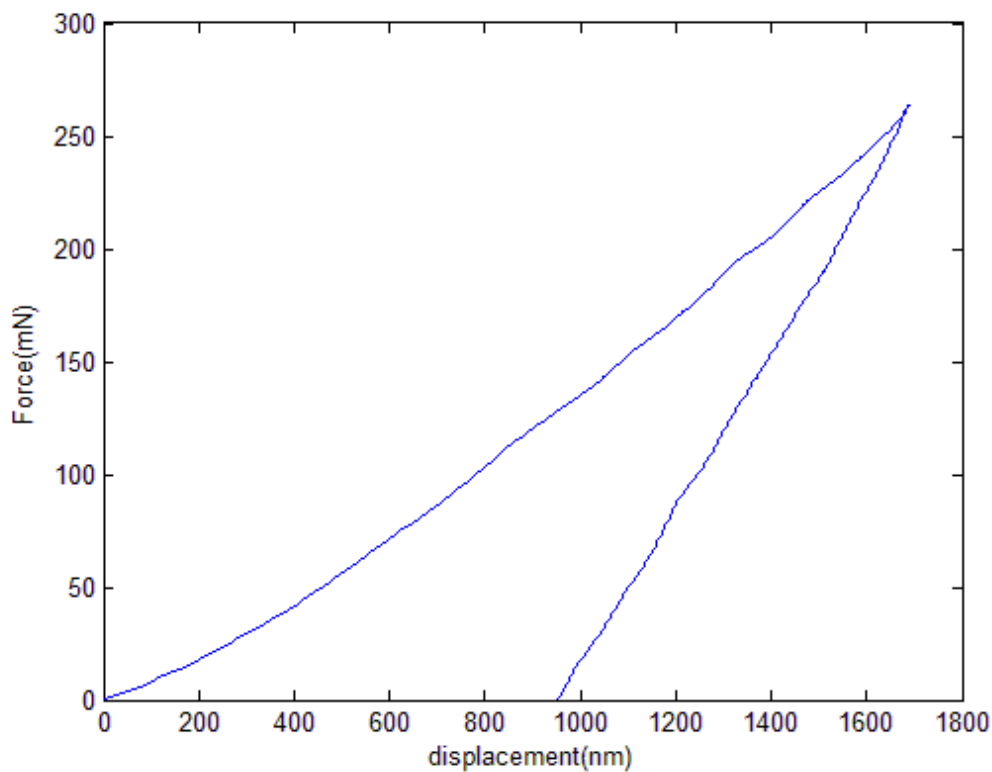


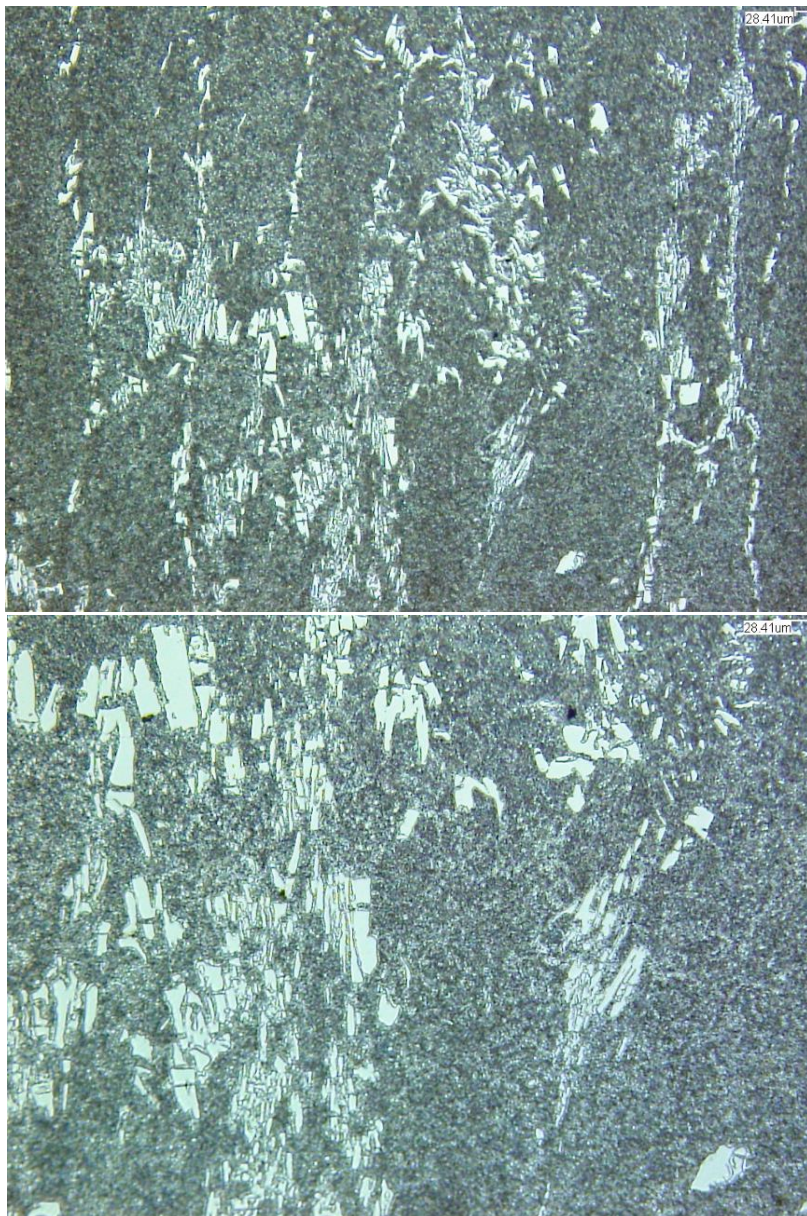
Fig.19. The force-displacement wave in a completed nano-indentation

As shown in Fig.19, the left side of curve is the in the loading period and the right side of the curve is the unloading. In the loading period, it has the loading elasticity, elasticity-plasticity and plasticity, while, in the unloading curve, it has the unloading elasticity, elasticity-plasticity and plasticity.

Chapter 4 Experimental results

By the nano-indentation system has been set up, to test the elasticity and plasticity for a material would process. In this experiment, it indents the D2 steel, which is the tooling material. It is a hard material and has the low tensile ability. For it has the big size of the carbide, which is carbide, indent it and determine the plasticity and elasticity of it would be in the experiment.

4.1 Microstructure of the material



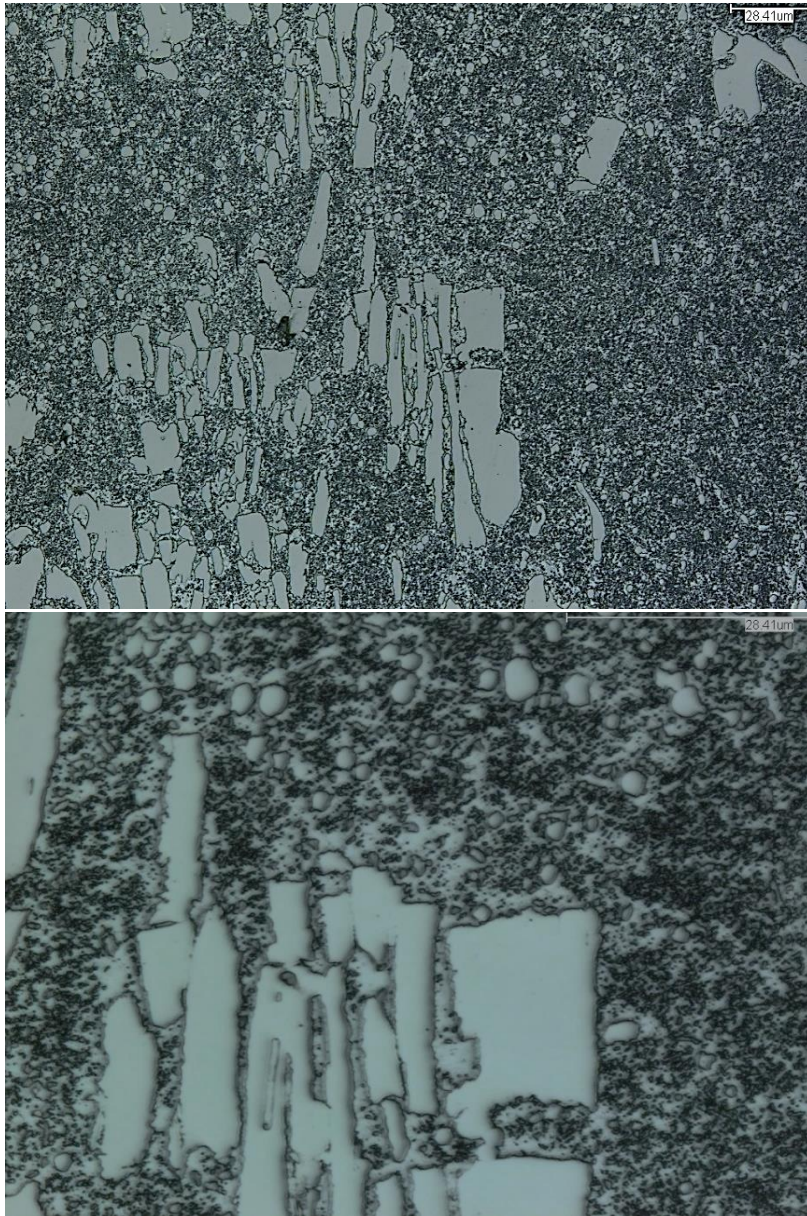


Fig.20. The microstructure of D2 in 200X (1st), 400X (2nd), 1000X (3rd) and 3000X (4th) microscope (provided by Pengyan Lu)

After polishing and etching D2, the material puts in the telescope and determines the martensite and the carbide. The specimen puts under the telescope which is in 10X, 20X, 50X and 150X. In the 10 fold microscope, it is obvious that the white component is the carbide and the black component is the martensite particles. In putting under the 20 fold telescope, the carbide is bigger than 28.4 micro * 28.4 micro. By using the laser scanning the specimen in 50

and 150 fold, the carbide are clear. By using the nano-indenter, it is easy to indent the whole indentation in the carbide. There are some boundaries between the martensite particles.

In this experiment, it is aim to indent on different kinds of particles and on the boundaries between two particles. In this experiment, indent on the carbide, martensite and boundaries would get material properties. For it is the blind indentation system, it needs to indent plenty of indentation for a big amount of area. Indent as many point as possible would collect more data. By doing the statistics for three particles, it would determine the global material properties.

4.2 Microscope after the indentation

In Fig.21, there are 150 indentation points on the specimen. Each deformation of the specimen is 10 micrometers, which would make less affects among these indentation points. For is has mentioned that this is the blind indentation system, thus some of the points are on the carbide, however, the rest of them are on the martensite and on the boundaries.

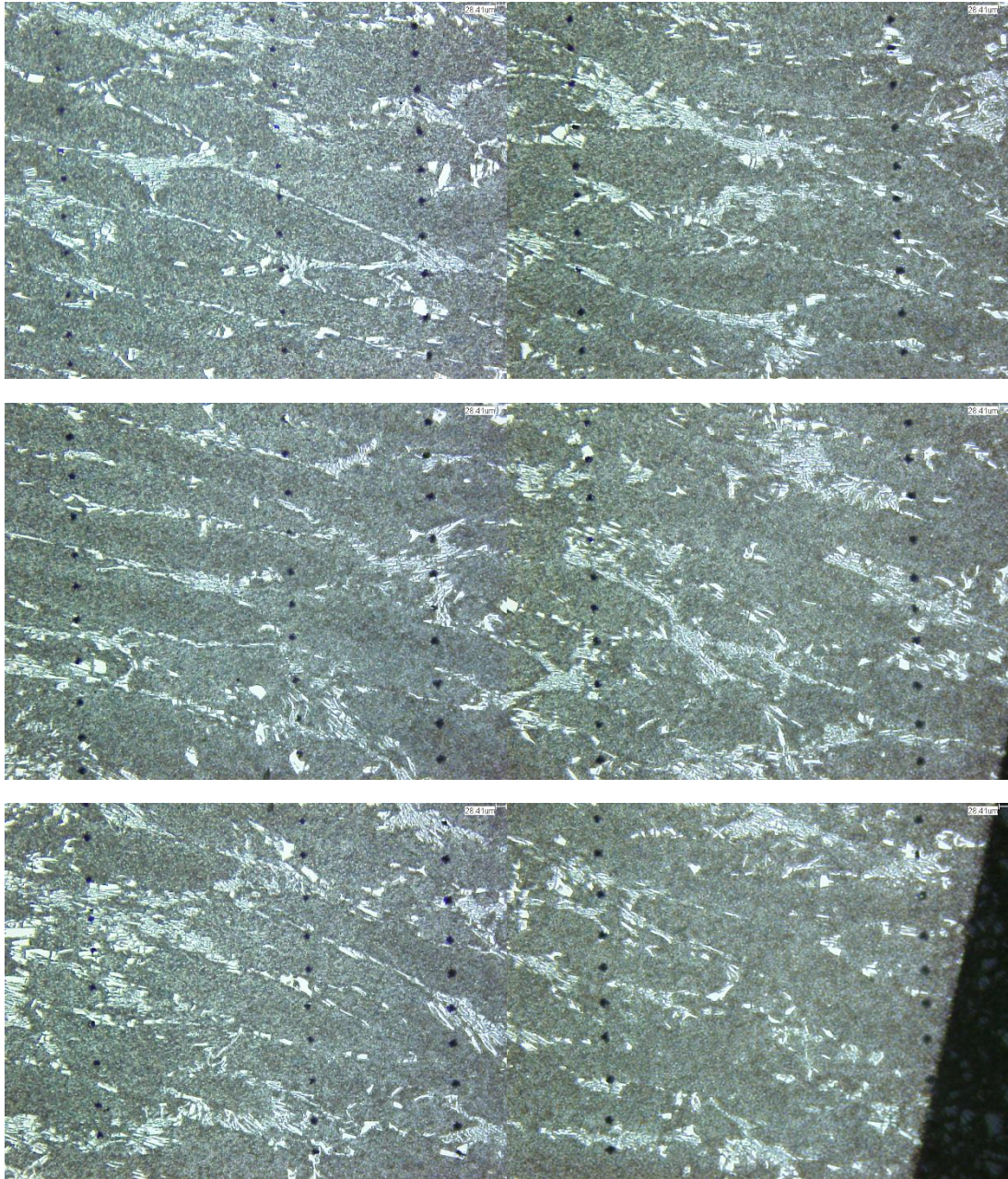


Fig.21. The microstructure of D2 after indentation in 200X microscope

There are 5 lines of the points on the specimen. By figuring out the number of the points on the carbide and on the boundaries, the density of the effective points would be clear.

Table 7. The statistics of the indentation on the carbide, the boundaries and the martensite

		On carbide	On boundaries	On martensite
Total (148 points)	Number	20	35	93
	Percent	13.5%	23.6%	62.9%

By the statistics, it has 13.5% of the indentations are on the carbide, 23.6% of the indentations are on the boundaries and 62.9% are on the martensite.

Simply set the half size of the indentation on the boundaries as carbide and another half belongs to martensite, thus the carbide consists of 32.5 indentations and 105.5 indentations belong to martensite. It could say 75% of the area is the martensite and 25% of the area is the carbide.

It randomly chooses 10 points on the carbides, 10 points on the boundary and 20 points on the martensite to determine the global material properties. By numbering 40 indentation points in line and column, it is easy to figure out the microstructure with the force-displacement curve.

For dividing 148 points into 3 particles, using the random function from the Matlab, it could get these 40 points randomly.

Table 8. Number the indentation points by each column and line

Carbide			Boundaries			Martensite					
No	Column	Line	No	Column	Line	No	Column	Line	No	Column	Line
1	1	17	11	2	7	21	1	3	31	3	13
2	1	25	12	2	29	22	1	15	32	3	19
3	2	3	13	3	29	23	1	28	33	3	20
4	2	30	14	4	2	24	2	3	34	4	7
5	3	16	15	4	18	25	2	9	35	4	9
6	3	23	16	5	5	26	2	15	36	4	21
7	3	26	17	5	9	27	2	16	37	4	22
8	3	30	18	5	13	28	2	27	38	5	3
9	4	24	19	5	17	29	3	2	39	5	5
10	5	1	20	5	23	30	3	4	40	5	9

For each indentation points have the number, then name each of the force-displacement wave is easier.

Firstly, collecting the force-displacement curve for the carbide, boundary and martensite. Then, comparing these 40 force-displacement curve and find the differences among them. Thirdly, determining the global force-displacement curve for 3 particles. Finally, obtaining the global material properties for these three particles.

4.3 Force-displacement wave for the particles

In the chapter 3, it has been told how to determine the force-displacement wave, which combines the force-time and displacement-time wave together by cohere the time line. The force-time wave and the displacement-time wave are both de-noised by the wavelet transform, which is in the dB4 window and by the 7 level of the de-noising.

4.3.1 Force-displacement wave for the carbide

For choosing the force-time and displacement-time wave for the carbide, these 10 indentation points for the carbide is determined.

For each carbide has one force-displacement curve, thus put them together and compare them would tell the global force-displacement curve for the carbide for this D2 steel. Firstly, convert the force-displacement curve from the raw data, and then put them in one plot one-by-one.

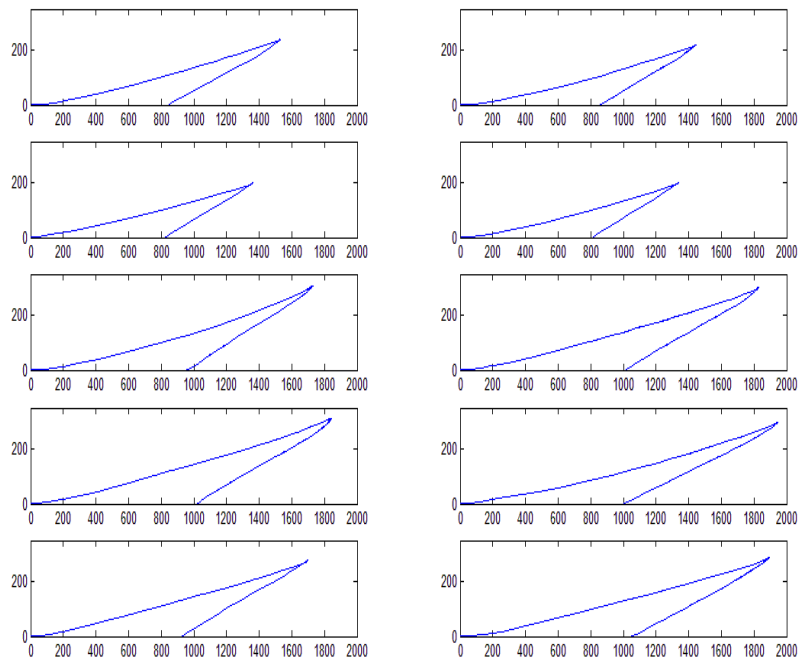


Fig.22. The indentation force-displacement wave for carbide

In these one-by-one wave, we could match each number of point in table.6 with the force-displacement wave in Fig.22. The wave in 1st line and 17th column is the No.1 indentation, the 1st line and 25th column wave is the No.2 indentation, and the rest can be done in the same manner.

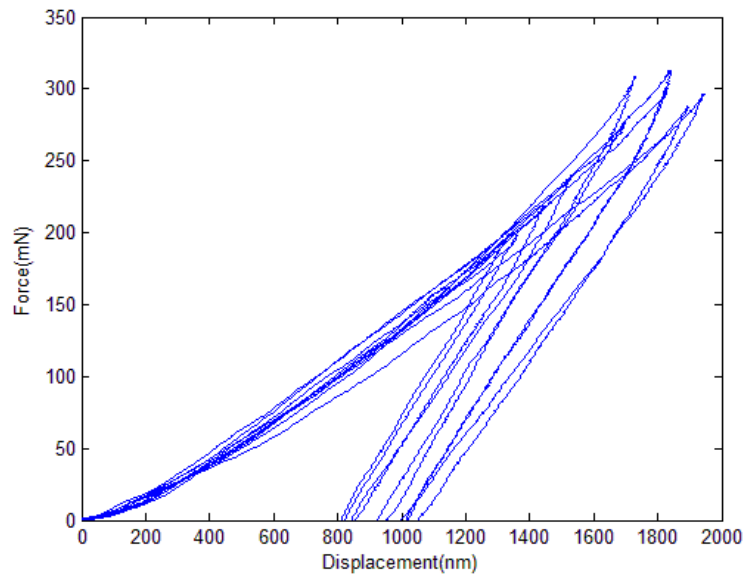


Fig.23. The force-displacement wave for 10 carbide indentation

For the wave in Fig.23 is separate, it is very hard to compare each indentation point to other indentation points. In fig.21, 10 pieces of the image are combined in one x-y-axis plot. The loading force for each indentation has some differences, so the displacement and deformation are different too.

For the force-displacement curve for the carbide has been determined, then it needs to see is there any differences with the boundaries and martensite.

4.3.2 Force-displacement wave for the boundaries

The same as 4.3.1, it uses the same way to convert the force-displacement curve for the boundary.

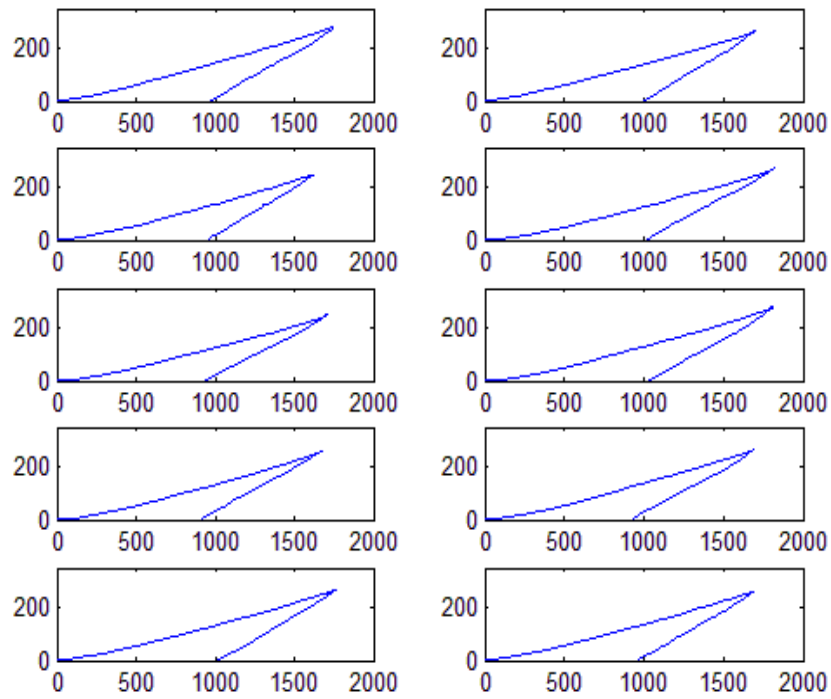


Fig.24. The indentation force-displacement wave for the boundary

In Fig.24, the 1st plot is the force-displacement wave for particle 11, the 2nd is for particle 12. The rest of the plots are in the same manner. Then combine these 10 plots in the same x-y plot to see if there are any differences with each other.

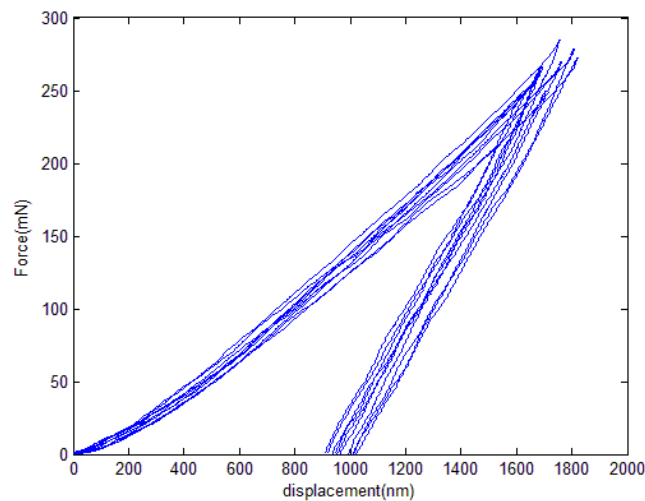


Fig.25. The force-displacement wave for 10 boundary indentation

The combination curve for the boundary is determined. Finally, it needs to calculate the curve for the martensite.

4.3.3 Force-displacement wave for martensite

Choosing 20 points from table 6 of the martensite, it uses the same way to convert the force-displacement curve.

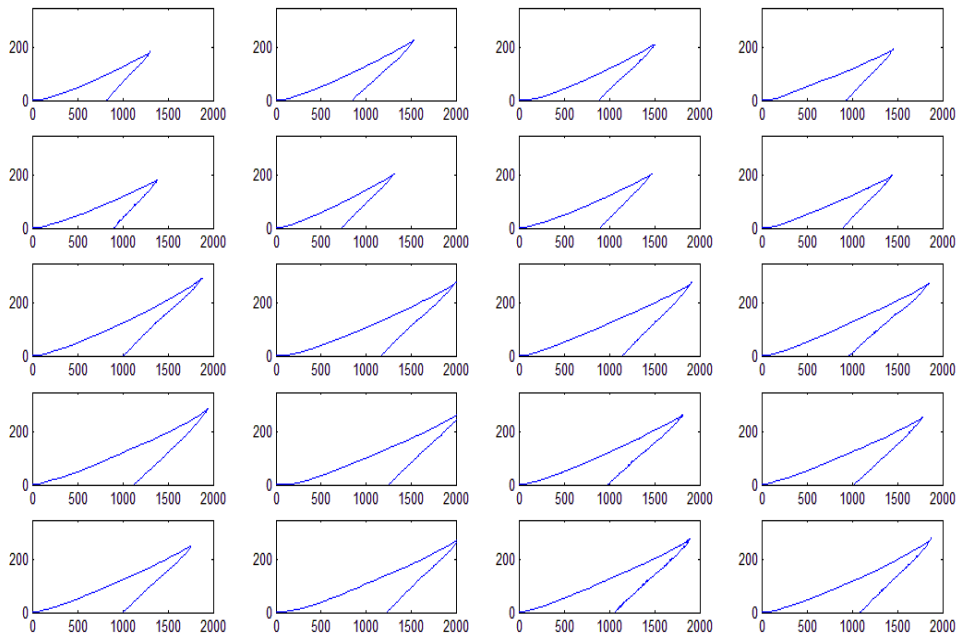


Fig.26. The indentation force-displacement wave for the martensite

Putting 20 plots in the same x-y axis, it would see is there any difference with 20 plots for the martensite?

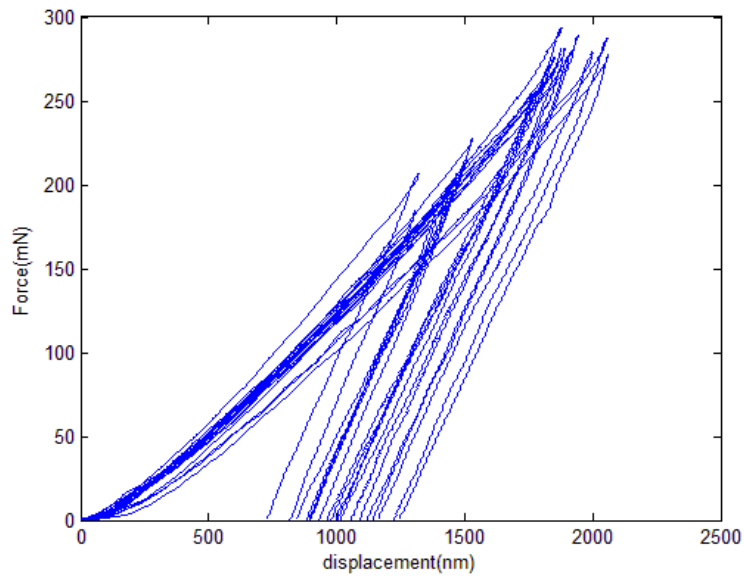


Fig.27. The force-displacement wave for 20 martensite indentation

The combination curve for the martensite is determined. With 3 combination plots for 3 kinds of particle, put them together and it would tell the differences with them.

4.3.4 Combination of force-displacement wave for particles

For all 40 particles has the force-displacement curve, then put them together into one x-y plot would tell the differences with carbide, boundary and martensite.

It has 40 curve to show the material properties for 3 kinds of particles, so the trends is able to tell their differences. If the slope is abrupt, it means the particle is hard. Otherwise, the gentle slope means the particle is soft.

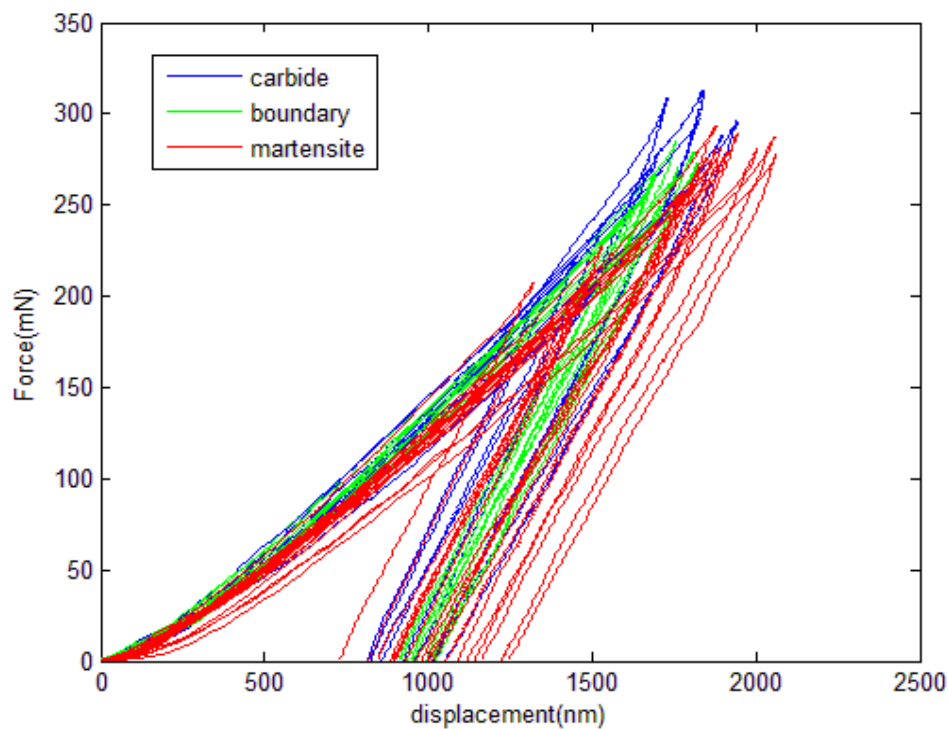


Fig.28. The force-displacement wave for carbide (blue), boundary (green) and martensite (red)

It is obvious that the slopes for most of the martensite are gentle, so this particle is soft than others. However, the carbide and the boundary are uneasy to tell the differences with each other.

For checking the microstructure for the carbide and boundary again, only the surface has been polished. Thus, under the boundary maybe still the carbide. So, the curves for the carbide are mixed with the boundary.

4.4 Analysis for the material properties for carbide, boundary and martensite

In 4.3, the force-displacement curves for 40 particles have been determined. By using the equation from chapter 2, the stain and stress for each force is able to use the function to do the calculation.

Firstly, it needs to find the maximum load P_{\max} , the maximum depth h_{\max} , the elastic recovery depth h_c , and the reminding depth h_f . With these data, it is able to know the hardness, stiffness, stain and stress for each force.

Table 9. P_{\max} , h_{\max} , h_c and h_f for the carbide, boundary and the martensite

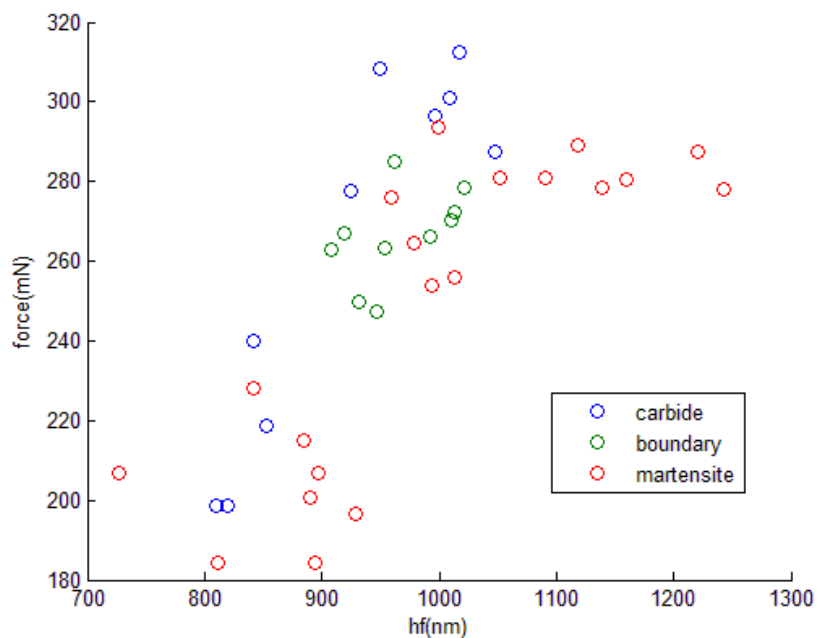
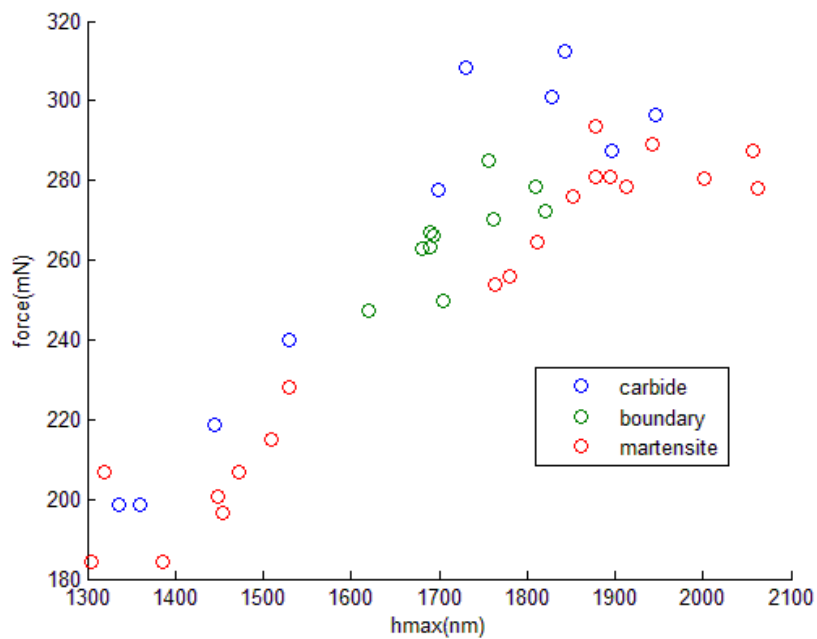
Carbide (unit for h_{\max} , h_c and h_f are nm, P_{\max} is mN)					Boundary (unit for h_{\max} , h_c and h_f are nm, P_{\max} is mN)				
No	P_{\max}	h_{\max}	h_f	h_c	No	P_{\max}	h_{\max}	h_f	h_c
1	239.91	1529.65	842.18	844.25	11	284.97	1756.74	962.33	962.89
2	218.76	1445.46	853.15	855.36	12	266.14	1694.03	991.78	992.89
3	198.53	1360.42	819.16	820.22	13	247.36	1619.92	946.60	947.84
4	198.69	1336.82	809.51	811.27	14	272.33	1820.68	1012.52	1013.85
5	308.38	1729.80	949.30	950.61	15	249.63	1705.16	932.06	933.29
6	300.78	1828.67	1009.53	1010.99	16	278.41	1808.80	1021.15	1022.18
7	312.40	1842.58	1017.15	1018.40	17	262.70	1680.48	908.73	910.01
8	296.42	1945.57	996.89	997.68	18	266.84	1690.04	918.70	919.52
9	277.61	1699.54	924.96	925.66	19	270.24	1761.91	1010.30	1011.34
10	287.61	1896.91	1048.16	1048.83	20	263.43	1689.04	953.47	954.28
Martensite (unit for h_{\max} , h_c and h_f are nm, P_{\max} is mN)									
No	P_{\max}	h_{\max}	h_f	h_c	No	P_{\max}	h_{\max}	h_f	h_c
21	184.44	1305.22	811.06	812.37	31	278.64	1912.25	1138.41	1139.40
22	227.92	1529.65	842.18	844.24	32	275.82	1851.74	958.83	959.99
23	214.90	1508.49	884.39	886.13	33	289.05	1942.41	1118.16	1119.30
24	196.61	1454.26	928.33	930.91	34	278.05	2061.54	1242.10	1243.93
25	184.19	1386.57	894.37	896.91	35	264.64	1812.12	978.91	980.23
26	206.82	1319.96	726.35	727.12	36	256.12	1779.41	1013.29	1015.09
27	206.78	1472.25	897.26	898.50	37	253.83	1763.19	993.45	994.08

28	200.84	1448.68	889.73	890.69	38	287.31	2057.34	1221.09	1222.42
29	293.54	1877.92	999.77	1001.15	39	281.07	1894.51	1051.39	1051.86
30	280.52	2002.24	1159.15	1160.39	40	281.06	1877.37	1090.36	1091.67

In the table 9, it tells us in which direct force, the h_{\max} , h_c and h_f would be in which depth.

Plot these data into h_{\max} -p, h_c -p and h_f -p and find the sequence. Three kinds of particles are put

in one plot, this is easy to figure out the sequence and differences



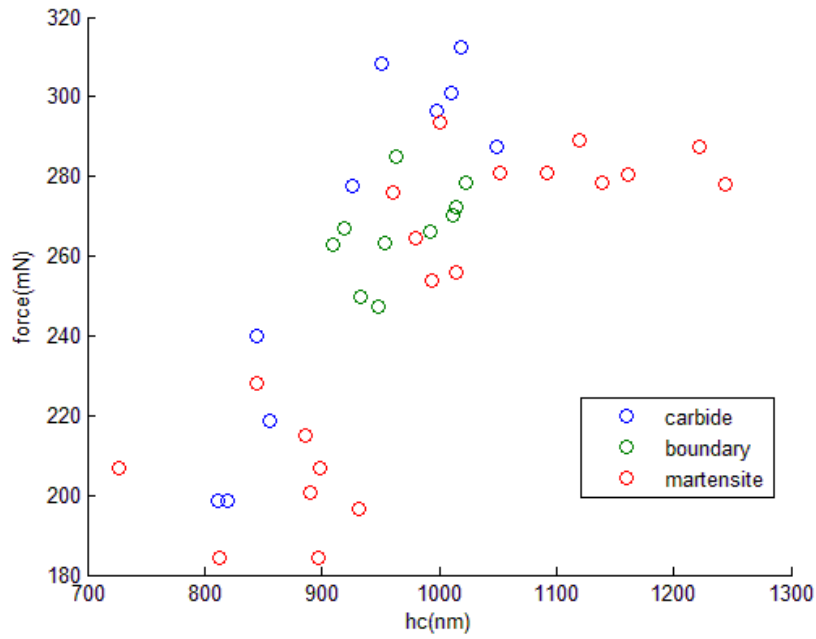


Fig.29. h_{\max} -p, h_c -p and h_f -p plot for the carbide, boundary and martensite

In Fig.29, it is obvious that martensite is the softest particle in these three kinds of particles.

The dots for the carbide are mixed with the boundaries. Thus it could prove that the particles under the boundaries are carbide.

With the P_{\max} , h_{\max} , h_c and h_f , it is able to know the hardness, stress and strain.

The effective stress distributes from equation 4. There are some of the unknowns, β , A_c and S . The β ratio in equation 6 is to obtain the indenter factor to distribute the stress. In the

equation, $\beta = \pi \frac{[\frac{\pi}{4} + 0.1548 \cot \varphi \frac{1-2\gamma}{4(1-\gamma)}]}{[\frac{\pi}{2} - 0.8312 \cot \varphi \frac{1-2\gamma}{4(1-\gamma)}]^2}$, γ is the Poisson ratio for the indenter, and φ is the

half angle for the tip of the indenter. The indenter is made of diamond and the tip is 60° , so

the factor β is 1.737. A_c is the cross section area between the indenter and the specimen. In

equation 2, we know that $A_c = \pi(\frac{\sqrt{3}}{3} h_c)^2$. S is the stiffness of the specimen, which is $S =$

$\frac{dP}{dh}$ in equation 1. So with solution of these unknowns, the effective stress is $S =$

$\beta \frac{2}{\sqrt{\pi}} E_{\text{eff}} \sqrt{A_c}$. The effective subtracts the stress for the indenter is the stress for the specimen.

In the equation $\frac{1}{E_{\text{eff}}} = \frac{1-\gamma^2}{E} + \frac{1-\gamma_i^2}{E_i}$, E is the stress for the specimen. $\varepsilon = \frac{a}{R} = \frac{h_c}{h_{\text{max}}}$ is to

get the strain for the specimen.

Table 10. The young's modulus, stain and stress for 3 particles for direct force

Carbide (unit stress is MPa, Y modulus is GPa)					Boundary (unit stress is MPa, Y modulus is GPa)				
No	P _{max}	Y modulus	strain	stress	No	P _{max}	Y modulus	strain	stress
1	239.91	646.96	0.55	411.19	11	284.97	396.8	0.55	353.21
2	218.76	623.90	0.59	419.98	12	266.14	274.08	0.59	379.18
3	198.53	621.03	0.60	414.48	13	247.36	377.44	0.59	386.72
4	198.69	625.52	0.61	424.02	14	272.33	271.06	0.56	351.55
5	308.38	649.38	0.55	392.17	15	249.63	334.34	0.55	329.34
6	300.78	620.58	0.55	384.17	16	278.41	371.9	0.57	352.51
7	312.40	624.75	0.55	388.59	17	262.70	303.16	0.54	364.55
8	296.42	622.50	0.51	342.22	18	266.84	401.96	0.54	362.67
9	277.61	651.98	0.54	397.55	19	270.24	270.53	0.57	351.08
10	287.61	600.19	0.55	363.21	20	263.43	335.82	0.56	367.08
Martensite (unit for stress is MPa, young's modulus is GPa)									
No	P _{max}	Y modulus	strain	stress	No	P _{max}	Y modulus	strain	stress
21	184.44	112.05	0.62	392.53	31	278.64	109.22	0.60	301.46
22	227.92	113.82	0.55	367.52	32	275.82	112.90	0.52	343.94
23	214.90	111.81	0.59	384.39	33	289.05	109.92	0.58	310.67
24	196.61	109.79	0.64	318.67	34	278.05	107.72	0.60	252.39
25	184.19	109.88	0.65	321.58	35	264.64	111.87	0.54	316.51
26	206.82	116.88	0.55	413.11	36	256.12	110.71	0.57	322.06
27	206.78	111.03	0.61	359.76	37	253.83	111.05	0.56	327.36
28	200.84	110.90	0.61	355.58	38	287.31	108.26	0.59	270.05
29	293.54	112.63	0.53	336.56	39	281.07	110.92	0.56	325.56
30	280.52	108.95	0.58	296.37	40	281.06	110.15	0.58	331.24

For table 10, it could tell us the young's modulus, strain and stress in the maximum loading for carbide, boundary and martensite for some number of the force. By plot the strain-stress dot for each kinds of particles, it would tell some sequences.

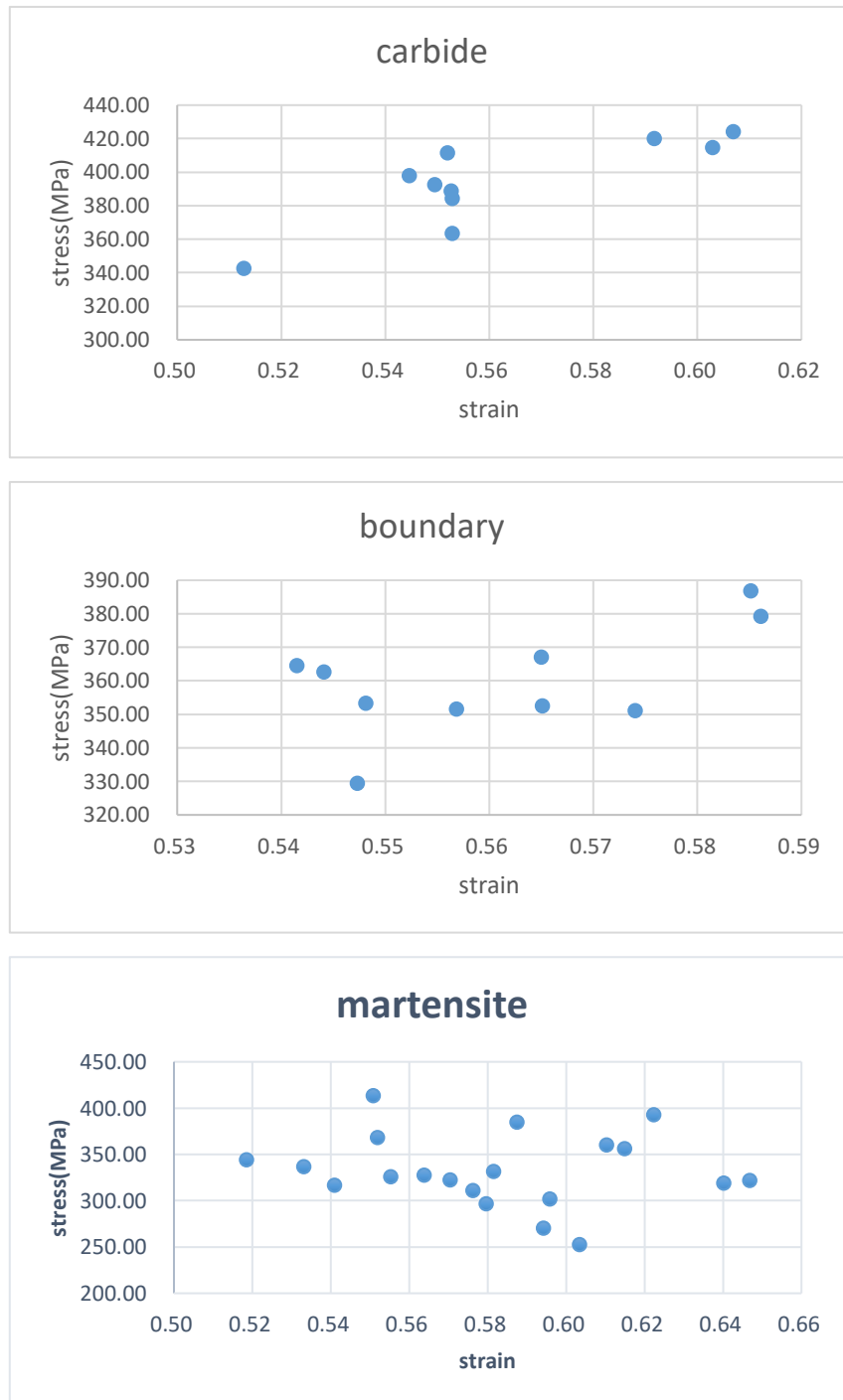


Fig.30. The strain-stress scatter for the carbide, boundaries and martensite

For the carbide and boundaries, the trends for the strain-stress moving is very clear. When

the strain increase, the stress does also increase. However, for the martensite, this trends is not obvious. This condition happens, it may have some impurities in the martensite. But what is the reason, it would be the future work.

Chapter 5 Future work

It is only obtained the material elastic properties so far and not able to evaluate the plastic properties because of the stress-strain curve needs to be determined through the FEA model during the loading period. Once the empirical formula describing the relationship between stress and strain for this indenter is established, the plasticity for each indentation would be easily assessed.

Chapter 6 Conclusion

This customized nano-indentation system is properly developed by designing the hardware arrangement, selecting the controlling mode and processing the collected signal.

This developed nano-indentation system is verified by testing AISI D2 steel. Based on the generated force-displacement curve of entire indentation period, the elastic properties of individual particles including Young's modulus and hardness are evaluated. It is obtained that the averaged Young's modulus of martensite, carbide and boundary are respectively 111GPa, 628GPa and 333GPa, and that the mean hardness of martensite, carbide and boundary are separately 13GPa, 18GPa and 15GPa.

APPENDIX

In the appendix is the code to do the controlling system and data processing.

Controlling system:

```
function varargout = MotorControl_0502(varargin)

% MOTORCONTROL_0502 M-file for MotorControl_0502.fig

%     MOTORCONTROL_0502, by itself, creates a new MOTORCONTROL_0502 or
raises the existing

%     singleton*.

%     H = MOTORCONTROL_0502 returns the handle to a new
MOTORCONTROL_0502 or the handle to

%     the existing singleton*.

%%     MOTORCONTROL_0502('CALLBACK', hObject, eventData, handles, ...)
calls the local

%     function named CALLBACK in MOTORCONTROL_0502.M with the given
input arguments.

%     MOTORCONTROL_0502('Property','Value',...) creates a new
MOTORCONTROL_0502 or raises the

%     existing singleton*. Starting from the left, property value
pairs are

%     applied to the GUI before MotorControl_0502_OpeningFcn gets
called. An
```

```

% unrecognized property name or invalid value makes property
application

% stop. All inputs are passed to MotorControl_0502_OpeningFcn via
varargin.

% *See GUI Options on GUIDE's Tools menu. Choose "GUI allows only
one

% instance to run (singleton)".

% See also: GUIDE, GUIDATA, GUIHANDLES

% Edit the above text to modify the response to help MotorControl_0502

% Last Modified by GUIDE v2.5 02-May-2015 13:04:31

% Begin initialization code - DO NOT EDIT

gui_Singleton = 1;

gui_State = struct('gui_Name',      mfilename, ...

                  'gui_Singleton', gui_Singleton, ...

                  'gui_OpeningFcn', @MotorControl_0502_OpeningFcn, ...

                  'gui_OutputFcn', @MotorControl_0502_OutputFcn, ...

                  'gui_LayoutFcn', [] , ...

                  'gui_Callback',  []);

if nargin && ischar(varargin(Adams, Malone Gill Productions. et al.))

    gui_State.gui_Callback = str2func(varargin(Adams, Malone Gill
Productions. et al.));

```

```

end

if nargin

    [varargout(Shyi-Ming)] = gui_mainfcn(gui_State, varargin(Veenis,
Stichting Historie der Techniek. et al.));

else

    gui_mainfcn(gui_State, varargin(Veenis, Stichting Historie der
Techniek. et al.));

end

% End initialization code - DO NOT EDIT

% --- Executes just before MotorControl_0502 is made visible.

function MotorControl_0502_OpeningFcn(hObject, eventdata, handles,
varargin)

% This function has no output args, see OutputFcn.

% hObject    handle to figure

% eventdata  reserved - to be defined in a future version of MATLAB

% handles    structure with handles and user data (see GUIDATA)

% varargin   command line arguments to MotorControl_0502 (see VARARGIN)

% Choose default command line output for MotorControl_0502

handles.output = hObject;

% Update handles structure

guidata(hObject, handles);

```

```

% UIWAIT makes MotorControl_0502 wait for user response (see UIRESUME)

% uiwait(handles.figure1);

% --- Outputs from this function are returned to the command line.

function varargout = MotorControl_0502_OutputFcn(hObject, eventdata,
handles)

% varargout cell array for returning output args (see VARARGOUT);

% hObject handle to figure

% eventdata reserved - to be defined in a future version of MATLAB

% handles structure with handles and user data (see GUIDATA)

% Get default command line output from handles structure

varargout(Adams, Malone Gill Productions. et al.) = handles.output;

% --- Executes on button press in Start.

function Start_Callback(hObject, eventdata, handles)

% hObject handle to Start (see GCBO)

% eventdata reserved - to be defined in a future version of MATLAB

% handles structure with handles and user data (see GUIDATA)

clear; close all; clc;

global Vertical_Control; % make h a global variable so it can be used
outside the main

% function. Useful when you do event handling and sequential
move

```

```

global Horizontal_Control;

%% Create Matlab Figure Container

fpos    = get(0,'DefaultFigurePosition'); % figure default position

fpos(3) = 1300; % figure window size;Width

fpos(4) = 450; % Height

f = figure('Position', fpos,...

           'Menu','None',...

           'Name','APT GUI');

%% Create ActiveX Controller

Vertical_Control = actxcontrol('MGMOTOR.MGMotorCtrl.1',[20 20 600

400 ], f);

Horizontal_Control = actxcontrol('MGMOTOR.MGMotorCtrl.1',[650 20 600

400 ], f);

Vertical_Control.methods('-full')

Horizontal_Control.methods('-full')

%% Initialize

% Start Control

Vertical_Control.StartCtrl;

Horizontal_Control.StartCtrl;

% Set the Serial Number

SN = 63001314; % put in the serial number of the hardware

```

```
set(Vertical_Control,'HWSerialNum', SN);

SN = 63001325; % put in the serial number of the hardware

set(Horizontal_Control,'HWSerialNum', SN);

samplingRate = 100;

numberOfSamples = 1;

inputRange = [-15,15];

excelFileName = 'sampleData';

AI = analoginput('nidaq','Dev1');

addchannel(AI,0);

set(AI,'InputType','SingleEnded');

%start(AI);

%data=getdata(AI);

% Identify the device

Vertical_Control.Identify;

Horizontal_Control.Identify;

%Jog Mode setting

Vertical_Control.SetJogMode(0,2,1);

Vertical_Control.SetJogStepSize(0,0.0005);

Horizontal_Control.SetJogMode(0,2,1);

Horizontal_Control.SetJogStepSize(0,0.01);

%Get Forward and Rearward movement limit
```



```
Ver_Motor_Min_Limit =  
  
0.; %Vertical_Control.GetStageAxisInfo_MaxPos(0,0);  
  
Ver_Motor_Max_Limit =  
  
1.; %Vertical_Control.GetStageAxisInfo_MinPos(0,0);  
  
Hori_Motor_Min_Limit =  
  
2.; %Vertical_Control.GetStageAxisInfo_MaxPos(0,0);  
  
Hori_Motor_Max_Limit =  
  
3.; %Vertical_Control.GetStageAxisInfo_MinPos(0,0);  
  
% Move a absolute distance  
  
Ver_Current_Position = Vertical_Control.GetPosition_Position(0);  
  
Hori_Current_Position = Horizontal_Control.GetPosition_Position(0);  
  
data_low=0.0005;  
  
data_high= 0.008;  
  
Ver_high=7;  
  
Samplerate = 10000;  
  
Sampletrigger = 2000;  
  
time = 0;  
  
Ver_distance = 0;  
  
Ver_dis = 0;  
  
test_n = 0;  
  
fid=fopen('MyFile.txt','w');
```

```

start(AI);

data=getdata(AI);

data_average=mean(data);

data = 0;

while (data<data_low)

    Vertical_Control.MoveJog(0,2);

    Ver_Current_Position =

Vertical_Control.GetPosition_Position(0);

    set(AI, 'SampleRate', Samplerate);

    set(AI, 'SamplesPerTrigger', Sampletrigger);

    start(AI);

    data=getdata(AI)-data_average;

    data=mean(data);

    Ver_Limit_Position = Ver_Current_Position;

end

Ver_0 = Ver_Current_Position;

while ((data>=data_low) & (data<data_high))

    Vertical_Control.MoveJog(0,2);

    Ver_Current_Position =

Vertical_Control.GetPosition_Position(0);

    set(AI, 'SampleRate', Samplerate);

```

```

set(AI, 'SamplesPerTrigger', Sampletrigger);

start(AI);

data=getdata(AI)-data_average;

Ver_displacement = Ver_Limit_Position - Ver_Current_Position;

data_mean_test(test_n + 1)=mean(data);

data=mean(data);

Ver_distance_test(test_n + 1) = Ver_displacement;

test_n = test_n + 1;

end

Ver_Lim_low = Ver_Current_Position;

while(data >= data_low)

    Vertical_Control.MoveJog(0,1);

    Ver_Current_Position =

Vertical_Control.GetPosition_Position(0);

set(AI, 'SampleRate', Samplerate);

set(AI, 'SamplesPerTrigger', Sampletrigger);

start(AI);

data=getdata(AI)-data_average;

Ver_displacement = Ver_Limit_Position - Ver_Current_Position;

data_mean_test(test_n + 1)=mean(data);

data=mean(data);

```

```
Ver_distance_test(test_n + 1) = Ver_displacement;

test_n = test_n + 1;

end

while (Ver_Current_Position < Ver_Limit_Position + 0.2)

    Vertical_Control.MoveJog(0,1);

    Ver_Current_Position =

Vertical_Control.GetPosition_Position(0);

end

Ver_lim_high = Ver_Current_Position;

Ver_down = Ver_lim_high - Ver_Lim_low;

Horizontal_Control.SetAbsMovePos(0,1);

Horizontal_Control.MoveRelative(0,1==0);

Hori_Current_Position = Horizontal_Control.GetPosition_Position(0);

pause;

Vertical_Control.SetJogMode(0,2,1);

Vertical_Control.SetJogStepSize(0,0.002);

Ver_Current_Position = Vertical_Control.GetPosition_Position(0);

while ((Hori_Current_Position < Hori_Motor_Max_Limit) &

(Hori_Current_Position > Hori_Motor_Min_Limit))

    while (Ver_Current_Position >= Ver_Lim_low)
```

```

Vertical_Control.MoveJog(0,2);

Ver_Current_Position =

Vertical_Control.GetPosition_Position(0);

Ver_Limit_Position= Ver_Current_Position;

    end

    while (Ver_Current_Position < Ver_lim_high)

        Vertical_Control.MoveJog(0,1);

        Ver_Current_Position =

Vertical_Control.GetPosition_Position(0);

    end

    Horizontal_Control.SetAbsMovePos(0,1);

    Horizontal_Control.MoveRelative(0,1==0);

    Hori_Current_Position = Horizontal_Control.GetPosition_Position(0);

End

```

Force-displacement combine curve

```

clear all

clc

open dis_9.fig;

displacement = get(get(gca, 'Children'), 'YData');

open force_9.fig;

```

```
force = get(get(gca, 'Children'), 'YData');

force_min = min(force);

force = force - force_min;

force = force*16100;

% reverse the force plot

[peak_displacement, displacement_T] = max(displacement); %find the
biggest displacement and point

[a, displacement_length] = size(displacement); %find the length of
displacement

[peak_force, force_T] = max(force); %find the biggest force and point

[b, force_length] = size(force); %find the length of force

%set the left and right array

displacement_left = displacement(1:displacement_T-1);

displacement_right = displacement(displacement_T:displacement_length);

%find the min NO of the left and right array

displacement_left_min = min(displacement_left);

displacement_right_min = min(displacement_right);

%get the number of the left and right force array

number_force_left = force_T;

number_force_right = force_length - force_T +1;

% get the new array for displacement
```

```

number_force_left = number_force_left -1;

force_left = force(1:number_force_left);

force_right = force(force_T:end);

sample_left = number_force_left/displacement_T;

force_left_new = force_left(1:sample_left:end-1);

sample_right = number_force_right/(displacement_length-displacement_T);

force_right_new = force_right(1:sample_right:end);

force_new = [force_left_new force_right_new];

displacement = displacement(1:displacement_length - 1);

displacement = displacement-displacement(1,1);

displacement = displacement*10^8;

figure;

plot(displacement,force_new);

ylabel('Force (mN) ');

xlabel('displacement (nm) ');

% young's modulus

dis_max = max(displacement);

force_max = max(force);

stiff = force_max/(dis_max - displacement(end))*10^6;

effect_mod = stiff/1.737/2*sqrt(3)/displacement(end)*10^9;

```

REFERENCES

Adams, W. H., Malone Gill Productions., 10 Corporation., Channel Four (Great Britain), Nexus Communications Ltd. and Public Media Video (Firm) (1995). Glory and grandeur The machine and the garden. Nature perfected, the story of the garden programs 9-10. S.I., Public Media Video,.

Ang, S. F., T. Scholz, A. Klocke and G. A. Schneider (2009). "Determination of the elastic/plastic transition of human enamel by nanoindentation." Dental Materials **25**(11): 1403-1410.

Anoop Suraj, A., M. Francis, T. S. Kavya and T. M. Nirmal (2014). "Discrete wavelet transform based image fusion and de-noising in FPGA." Journal of Electrical Systems and Information Technology **1**(1): 72-81.

Antretter, T. and F. D. Fischer (1997). "Critical shapes and arrangements of carbides in high-speed tool steel." Materials Science and Engineering: A **224**(1): 6-11.

Badkar, D. S., K. S. Pandey and G. Buvanashakaran (2010). "Effects of laser phase transformation hardening parameters on heat input and hardened-bead profile quality of unalloyed titanium." Transactions of Nonferrous Metals Society of China **20**(6): 1078-1091.

Chen, W. (2014). "Computation of two-dimensional Fourier transforms for noisy band-limited signals." Applied Mathematics and Computation **246**: 199-209.

Chen, W., X. Su, Y. Cao, Q. Zhang and L. Xiang (2005). "Method for eliminating zero spectrum in Fourier transform profilometry." Optics and Lasers in Engineering **43**(11): 1267-1276.

Chen, Z., X. Wang, F. Giuliani and A. Atkinson (2014). "Surface quality improvement of porous thin films suitable for nanoindentation." Ceramics International **40**(3): 3913-3923.

Cho, K. T., K. Song, S. H. Oh, Y.-K. Lee and W. B. Lee (2014). "Enhanced surface hardening of AISI D2 steel by atomic attrition during ion nitriding." Surface and Coatings Technology **251**: 115-121.

Choudhury, S. K. and S. Chinchankar (2017). 1.3 Finish Machining of Hardened Steel A2 - Hashmi, MSJ. Comprehensive Materials Finishing. Oxford, Elsevier: 47-92.

Conci, M. D., A. C. Bozzi and A. R. Franco Jr (2014). "Effect of plasma nitriding potential on tribological behaviour of AISI D2 cold-worked tool steel." Wear **317**(1–2): 188-193.

Djurović, I. and L. Stanković (2012). "STFT-based estimator of polynomial phase signals." Signal Processing **92**(11): 2769-2774.

Dong-hai, W., J. Yue-song, Z. Yan-zhong and G. Qian (2014). "An adaptive nonlocal means filter based on fuzzy domain for laser speckle reduction." Optik - International Journal for Light and Electron Optics **125**(7): 1833-1836.

Ersen, O., I. Florea, C. Hirlimann and C. Pham-Huu (2015). "Exploring nanomaterials with 3D electron microscopy." Materials Today **18**(7): 395-408.

Fisher-Cripps, A. C. (2000). "Introduction to Contact Mechanics."

Fukai, J. and T. Ando (2004). "Microstructure development in alloy splats during rapid solidification." Materials Science and Engineering: A **383**(1): 175-183.

Hamilton, N. R., J. Wood, A. Galloway, M. B. Olsson Robbie and Y. Zhang (2013). "The metallurgy, mechanics, modelling and assessment of dissimilar material brazed joints."

Journal of Nuclear Materials **432**(1): 42-51.

Hane, K. F. and T. W. Shield (2000). "Microstructure in the cubic to trigonal transition."

Materials Science and Engineering: A **291**(1–2): 147-159.

Hay, J. C., A. Bolshakov and G. M. Pharr (1999). "A critical examination of the fundamental relations used in the analysis of nanoindentation data." Journal of Materials Research **14**(6): 2296-2305.

Hutchings, I. M. (2009). "The contributions of David Tabor to the science of indentation hardness." Journal of Materials Research **24**(3): 581-589.

Kanari, M., K. Tanaka, S. Baba and M. Eto (1997). "Nanoindentation behavior of a two-dimensional carbon-carbon composite for nuclear applications." Carbon **35**(10–11): 1429-1437.

Karlsson, P., A. Gård and P. Krakhmalev (2014). "Influence of tool steel microstructure on friction and initial material transfer." Wear **319**(1): 12-18.

Kim, Y., T.-H. Ahn, D.-W. Suh and H. N. Han (2015). "Variant selection during mechanically induced martensitic transformation of metastable austenite by nanoindentation." Scripta Materialia **104**: 13-16.

La Torre, D. and E. R. Vrscay (2014). "Fourier transforms of measure-valued images, self-similarity and the inverse problem." Signal Processing **101**: 11-18.

Liskiewicz, T., K. Kubiak and T. Comyn (2017). "Nano-indentation mapping of fretting-induced surface layers." Tribology International **108**: 186-193.

Liu, L., C. L. P. Chen, Y. Zhou and X. You (2015). "A new weighted mean filter with a two-

phase detector for removing impulse noise." Information Sciences **315**: 1-16.

Liu, L. and D. Mandler (2014). "Patterning carbon nanotubes with silane by scanning electrochemical microscopy." Electrochemistry Communications **48**: 56-60.

Liverani, E., A. H. A. Lutey, A. Ascari, A. Fortunato and L. Tomesani (2016). "A complete residual stress model for laser surface hardening of complex medium carbon steel components." Surface and Coatings Technology **302**: 100-106.

Machaka, R., T. E. Derry and I. Sigalas (2014). "Room temperature nanoindentation creep of hot-pressed B6O." Materials Science and Engineering: A **607**: 521-524.

Martínez, E., J. Romero, A. Lousa and J. Esteve (2003). "Nanoindentation stress–strain curves as a method for thin-film complete mechanical characterization: application to nanometric CrN/Cr multilayer coatings." Applied Physics A **77**(3): 419-427.

Nanesa, H. G., J. Boulgakoff and M. Jahazi (2016). "Influence of prior cold deformation on microstructure evolution of AISI D2 tool steel after hardening heat treatment." Journal of Manufacturing Processes **22**: 115-119.

Okonkwo, P. C., G. Kelly, B. F. Rolfe and M. P. Pereira (2012). "The effect of temperature on sliding wear of steel-tool steel pairs." Wear **282**: 22-30.

Oliver, W. C. and G. M. Pharr (1992). "An improved technique for determining hardness and elastic modulus using load and displacement sensing indentation experiments." Journal of Materials Research **7**(6): 1564-1583.

Paul, A. and M. Strano (2016). "The influence of process variables on the gas forming and press hardening of steel tubes." Journal of Materials Processing Technology **228**: 160-

169.

Poon, B., D. Rittel and G. Ravichandran (2008). "An analysis of nanoindentation in linearly elastic solids." International Journal of Solids and Structures **45**(24): 6018-6033.

Pradeepkumar, M. S., K. P. Sabin, N. Swain, N. Sridhara, A. Dey, H. C. Barshilia and A. K. Sharma (2015). "Nanoindentation response of ITO film." Ceramics International **41**(6): 8223-8229.

Saba, F., E. Kabiri, J. V. Khaki and M. H. Sabzevar (2016). "Fabrication of nanocrystalline TiC coating on AISI D2 steel substrate via high-energy mechanical alloying of Ti and C." Powder Technology **288**: 76-86.

Sam Paul, P., A. S. Varadarajan and R. Robinson Gnanadurai (2016). "Study on the influence of fluid application parameters on tool vibration and cutting performance during turning of hardened steel." Engineering Science and Technology, an International Journal **19**(1): 241-253.

Sebastiani, M., K. E. Johanns, E. G. Herbert and G. M. Pharr (2015). "Measurement of fracture toughness by nanoindentation methods: Recent advances and future challenges." Current Opinion in Solid State and Materials Science **19**(6): 324-333.

Shyi-Ming, C. (1997). "A new method for tool steel materials selection under fuzzy environment." Fuzzy Sets and Systems **92**(3): 265-274.

Spangel, S., E. Matthaiei-Schulz, A. Schulz, H. Vettters and P. Mayr (2002). "Influence of carbon and chromium content and preform shape on the microstructure of spray formed steel deposits." Materials Science and Engineering: A **326**(1): 26-39.

Staia, M. H., Y. Pérez-Delgado, C. Sanchez, A. Castro, E. Le Bourhis and E. S. Puchi-Cabrera (2009). "Hardness properties and high-temperature wear behavior of nitrided AISI D2 tool steel, prior and after PAPVD coating." Wear **267**(9): 1452-1461.

Starling, C. M. D. and J. R. T. Branco (1997). "Thermal fatigue of hot work tool steel with hard coatings." Thin Solid Films **308–309**: 436-442.

Stratton, P., C. H. Surberg and K. Lingenhöle (2008). "The effect of some heat treatment parameters on the dimensional stability of AISI D2." Cryogenics **48**(1): 42-47.

Swain, M. V. and J. T. Hagan (1976). "Indentation plasticity and the ensuing fracture of glass." Journal of Physics D: Applied Physics **9**(15): 2201.

Tiwari, A. and L. H. Hihara (2014). "Nanoindentation and morphological analysis of novel green quasi-ceramic nanocoating materials." Progress in Organic Coatings **77**(7): 1200-1207.

Ugweje, O. C. (2004). "Selective noise filtration of image signals using wavelet transform." Measurement **36**(3–4): 279-287.

Veenis, M., Stichting Historie der Techniek., OAPEN. and DOAB: Directory of Open Access Books. (2012). Material fantasies expectations of the western consumer world among the East Germans. Technology and European history series 6. Amsterdam, Amsterdam University Press,: 280 p.

Watanabe, H., S. Arase, T. Yamamoto, P. Wells, T. Onishi and G. R. Odette (2016). "Hardening and microstructural evolution of A533b steels irradiated with Fe ions and electrons." Journal of Nuclear Materials **471**: 243-250.

Yang, Z. (2014). "Collins formula interpreted as wavelet transform." Optik - International Journal for Light and Electron Optics **125**(13): 3181-3183.

Yu, X., N. A. Burnham and M. Tao (2015). "Surface microstructure of bitumen characterized by atomic force microscopy." Advances in Colloid and Interface Science **218**: 17-33.

ABSTRACT**DEVELOPMENT OF A NANO-INDENTATION SYSTEM AND APPLIED TO AISI D2 TESTING**

by

TANGYUE WU**AUGUST, 2017****Advisor:** Dr. Xin Wu**Major:** Mechanical Engineering**Degree:** Master of Science

Nano-indentation is a testing method to obtain variety of material properties applied to small volumes. (Poon, Rittel et al. 2008) (Poon, Rittel et al. 2008) (Poon, Rittel et al. 2008) It is common to use nano-indentation method to test material properties under the indenter that is close to or smaller than the scale of material constituents such as grains and phase particles.

In this thesis a simplified nano-indentation system is designed and developed, at much reduced cost and with the required function used for current study of dual phase advanced high strength steels containing martensite matrix and carbide particles at the scale of 20 μ m. From obtained force-displacement curves over individual phases the elastic and plastic properties of the phase can be obtained. This lab system has been used for analyzing the constituent properties of D2 materials, which is helpful for understanding the tool strength and microstructure damage during forming and trimming of recent advanced high strength materials.

AUTOBIOGRAPHICAL STATEMENT

I come from China and major in Industrial Engineering in the university. I change the major to the Mechanical Engineering which provides the strong background to my career. In the master years, I learnt a lot from professors, who are very kind and helpful. I learnt how to choose and arrange the hardware and software to fulfill the project. Indeed, I applied some of my knowledge into my internship and helped the company improve the work efficiency.

I am very thanking to Wayne State University and the professor. I will devote myself into the industry by what I learnt.